SunFlow: Water Quality Sampling in Jackson Blue Springs for Water Resource Management Using SUNFISH Autonomous Underwater Vehicle

FINAL REPORT

*Prepared by Patricia Spellman and Sunfish Inc. for the **Florida Department of Environmental Protection***

FDEP PROJECT: AT017

2024

TABLE OF CONTENTS

TABLE OF FIGURES

TABLES

EXECUTIVE SUMMARY

The Florida Department of Environmental Protection (FDEP) funded enhancements to an Autonomous Underwater Vehicle (AUV), SUNFISH, to support collecting water quality data and mapping the location and physical properties of karst conduits within the Floridan Aquifer System (FAS). These data collection efforts can be used to improve the effectiveness of state mandated water resource initiatives in Florida by informing land management decisions, improving groundwater modeling efforts, and expanding knowledge of flow and pollutant transport. The funding provided by the DEP for fiscal year 2023-2024 was for the integration and field-testing phase (Phase 1a) of a planned multi-part project and included 1) instrumenting SUNFISH with a SeaBird Scientific Submersible Ultraviolet Nitrate Analyzer (SUNA) V2 sensor 2) updating SUNFISH georeferencing capabilities for geospatial software integration, and 3) testing these new features in a phreatic cave system. In addition to testing the new features and delivering georeferenced nitrate concentrations, previously integrated technology on SUNFISH would be used to collect conduit data and develop a three-dimensional (3-D) conduit map, take high resolution video at key moments of feature testing, and monitor continuous salinity and temperature data.

The new feature testing and data collection was performed at Jackson Blue Spring. Originally, testing the new features on SUNFISH was going to be tested at Wakulla Springs, however, sustained high-flow conditions precluded AUV and diver operations during the available deployment window. As the deployment window approached, the team assessed numerous alternate deployment sites, and determined that, with high flow conditions prevailing at sites of interest across the state and rainy weather continuing in the forecast, Jackson Blue Spring remaining as the only viable option in the available schedule window. Though flow velocities and tunnel diameters at this site were not expected to allow for optimal tunnel mapping behaviors, the decision to deploy was made in consultation with DEP and Florida Geological Survey (FGS) to ensure that the field testing of the integrated nitrate sensor and georeferencing system, which were the focus of the project, could take place in the available timeline.

The first primary objective to integrate and field test the SUNA nitrate sensor was successful, as was the validation of the previously integrated conductivity and temperature sensor on SUNFISH. Validation of nitrate took place by collecting discrete water samples at three locations alongside SUNFISH which included the spring vent and two locations inside the cave. The water samples were analyzed at a National Environmental Laboratory Accreditation (NELAC) laboratory, and the SUNA nitrate sensor readings were within 10% of laboratory analyzed

samples; which is within the error expected of the SUNA sensor. Further, an increasing nitrate trend from the spring vent to 420 m inside the cave was observed from the laboratory nitrate samples, which was also detected by the SUNA nitrate sensor. High resolution video was recorded of water sampling performed by cave divers at the two sample sites inside the cave and delivered as supplemental data. The previously integrated Neil Brown Ocean Sensors Incorporated (NBOSI) temperature and conductivity sensor on SUNFISH was also validated. Temperature was validated with a National Institute of Science and Technology (NIST) calibrated thermometer and SUNFISH NBOSI temperature readings were within 2% of NIST thermometer readings. Calibration of the SUNFISH NBOSI conductivity was performed prior to deployment, however conductivity was also field validated by comparing NBOSI conductivity readings with two different and calibrated conductivity sensors; a YSI EXO^2 mounted conductivity/temperature sensor and a vanEssen conductivity, temperature, and depth (CTD) sensor. The readings between the YSI EXO^2 conductivity sensor and SUNFISH NBSOI conductivity were within the expected errors for the NBOSI sensor (20 µS/cm). However, temperature anomalies observed from the vanEssen may have caused some of the observed offset outside the error range (>20 µS/cm) in conductivity between the vanEssen and NBOSI sensor. Thus, there was more confidence in the YSI EXO^2 sensor readings and validation was confirmed.

The 3-D cave mapping and integration of the georeferencing feature was successful, but more work is needed to improve the uncertainty in the mapped location of the cave. A 3-D conduit map was generated for the first ~420 m (1450') of Jackson Blue cave. Unfortunately, minimum diameter restrictions and flow velocities that exceeded the limit for normal mapping operations by 250% were outside the specifications for SUNFISH to achieve high-resolution, full-accuracy mapping. To overcome the excessive flow velocity, the Sunfish team developed the "Gator Roll" in the field, which is a new vehicle behavior for this project to enable minimum viable sonar sensor coverage for mapping. While this behavior enabled traversing the cave and gathering sonar data around the entire tunnel circumference, it came at the cost of 3-D mapping resolution, which was reduced to ~1 m. It also could not address sources of significantly increased navigation error in the tunnel. Despite these challenges, mapping was completed and v ehicle navigation drift and resulting map 1σ uncertainty were quantified to 0.8 m at the entrance and up to 32.8 m at the maximum penetration limitThe uncertainties resulted from Doppler Velocity Log (DVL) time (12.3 m or 38%), DVL outages (11.3 m or 34%), heading (7.3 m or 22%), DVL distance (1.7 m or 5%), and the error in the Global Navigation Satellite System (GNSS) (0.2 m , 1%). Some of these uncertainties can be reduced with adjustments to mapping techniques, more conducive diameter and hydraulic conditions, and the use of control points to improve georeferenced navigation.

Therefore, as the Sunfish team works to improve vehicle features to reduce these uncertainties, sinkholes and karst windows that are common in many Florida cave systems and surveyed conduit wells can be used as control points to substantially reduce positional uncertainty. External validation techniques can also be employed to validate the map location such as radiolocation, which has been previously applied to caves in Florida and is currently being undertaken to validate the Jackson Blue cave map. The details of and current efforts to reduce these uncertainties are discussed in more detail throughout this report. Furthermore, work is continuing under an enhancement grant from the Defense Advanced Research Projects Agency (DARPA) to develop processing software which outputs georeferenced 3D voxel maps and nitrate data with quantitative error bounds.

Supplementing SUNFISH data collection was the collection and analysis of hydrogeochemical data from 5 springs that discharge to Merritt's Mill Pond; including Jackson Blue Spring. Merritt's Mill Pond is a lake sustained primarily by spring flow and nitrate concentrations in the pond have been increasing likely due to continued agriculture in the region (Katz, 2004), among other factors (Dodson, 2013). We collected nitrate (NO_3^- - N) and the $\delta^{18}O$ and $\delta^{15}N$ of nitrate to compare with previously collected isotope data and report any new insight from the new data collection. USF also independently, but simultaneously, collected other geochemical parameters including major ions (Ca^{2+}, Na^+, Mg^{2+}, K^+, SO_4^{2-}, Cl^-), alkalinity, water isotopes ($\delta^{18}O$, δ^2H), and some trace metals ($Fe^{2/3+}$, Mn^{2+}, Sr^+). The 5 springs where samples were collected included Jackson Blue Spring, Indian Washtub, Twin Caves, Hole-in the Wall, and Hidey Hole. The $\delta^{18}O$ and $\delta^{15}N$ isotopes revealed that the sources of nitrate pollution are similar to what has previously been reported (Katz, 2004, Barrios, 2011) which primarily implicate inorganic and organic fertilizers. Additional geochemical data also highlighted that springs discharging to the north section of the pond have distinctive water chemistries from those discharging from the south. These differences are likely due to both variations in geology and land use to the north and south of Merritt's Mill Pond. However, geochemical data also revealed one spring, Hole in the Wall, may discharge water that is a combination of flow from the north and south sections of the groundwater contributing area, as the mapped cave extends to the north and south of Merritt's Mill Pond.

The new enhancements coupled with previously field-tested capabilities haves positioned SUNFISH to be a valuable tool for researchers and water resource managers to collect data that improves our understanding of flow and transport in the Floridan Aquifer, which ultimately serves water resource management. Thus far, the ability to sample and collect high resolution data in phreatic caves has been restricted to cave divers, which have depth, time, and experience limitations. Therefore, limited water quality, physical, and hydrological data from these phreatic

caves has precluded significant advancements to groundwater quality and quantity remediation efforts. SUNFISH, however, can be used to improve these efforts and simultaneously answer critical research questions related to conduit hydraulics, nitrate variability and transformation, pollutant transport, and source water mixing that ultimately contribute to water quality changes in Florida's priority surface waters such as springs, rivers, and lakes.

PROJECT DESCRIPTION AND DELIVERABLES

The primary objectives in Phase 1a were to field-validate new capabilities on the SUNFISH vehicle, including integrating a nitrate sensor and improving map georeferencing capabilities This grant was also enhanced by the Department of Defense through a Defense Advanced Research Projects Agency (DARPA) grant to visualize the georeferenced water quality data using the ArcGIS 3D voxel layers feature (APPENDIX A) (https://geoxc-apps4.bd.esri.com/ocean-explorer/). Additionally, existing SUNFISH functionality was used to provide video of activities in the cave and generate 3-D conduit maps along with georeferenced water temperature and salinity. The following tables breakdown the total project costs and allotment (Table 1) followed by deliverables and their completion dates (Table 2).

Category	Grant Funding, Not to Exceed,$
Salaries Total	$13,975
Fringe Total	$3,412.15
Contractual Services Total	$528,000
Supplies	$100
Miscellaneous/Other Expenses	$2,700
Indirect Costs (F&A) Total	$11,297
Total DEP:	**$559,484.15**
Total DARPA:	**$159,988.00**

Table 1: Total project cost and the allotment and total DARPA funding.

DELIVERABLE	COMPLETED DATE
Georeferenced cave map and accuracy reporting	June 30, 2024
Cave map overlay on land use	June 30, 2024
Cave map overlay on DEM	June 30, 2024
Cave map and hydraulic gradients	**
Georeferenced nitrate, conductivity, temperature data	June 15, 2024

*Table 2: Deliverables for project AT017. ** Difficulties at the site made this deliverable challenging to obtain.*

BACKGROUND

The Floridan Aquifer System and karst hydrogeology

The Floridan Aquifer System (FAS) is one of the most productive aquifers in the United States (US) and is Florida's primary aquifer for water extractions; widely used for potable, agricultural, and industrial purposes. The FAS can be divided into upper and lower aquifers based on water quality and stratigraphy (Williams and Kuniansky, 2016), and these two divisions are known as the Upper Floridan Aquifer (UFA) and Lower Floridan Aquifer (LFA). However, the most extensive and explored phreatic cave systems are contained within the UFA and are breached and accessible where the UFA is hydrogeologically unconfined (Figure 1).

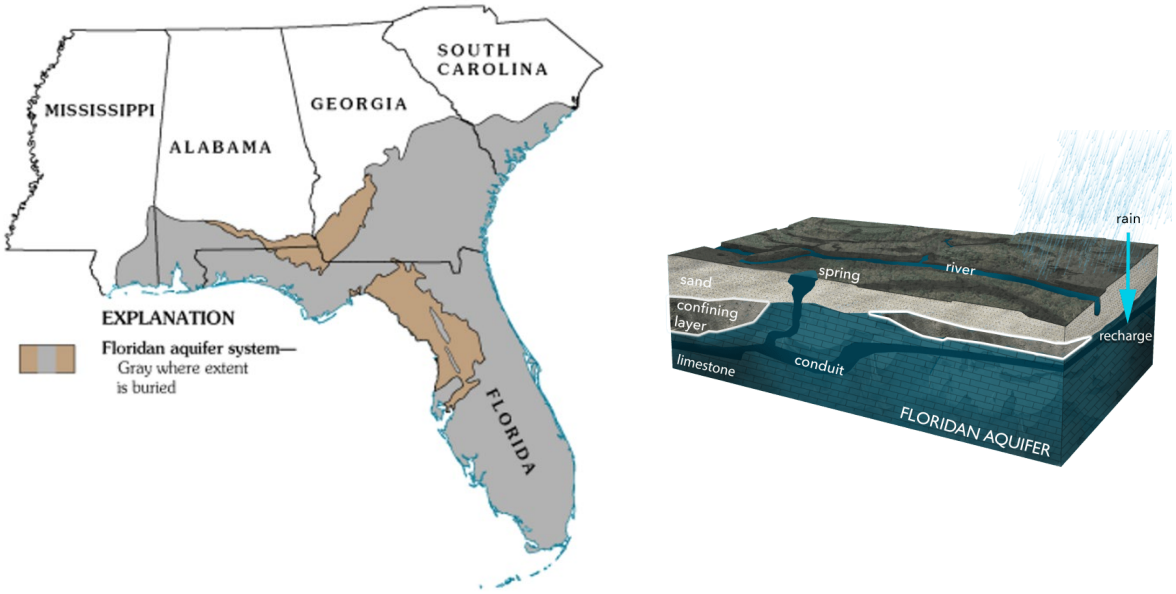

Figure 1: (Left) Extent of confinement for the Upper Floridan Aquifer (UFA). Star shows the approximate location of Jackson Blue Spring, the focus area of this report. (Right) FAS schematic with illustrations of diffuse recharge and conduit flow. Images retrieved from USGS.gov. Karst aquifers such as the FAS comprise variably integrated solutional porosity features that are embedded into a carbonate bedrock matrix (Ford and Williams, 2007). As karst aquifers evolve, solutional porosity features such as sinkholes, enlarged vadose fractures, and karst windows emerge that connect the land surface to the aquifer. After continued evolution, phreatic conduits enlarge and become the dominant pathway by which

groundwater and solutes are transmitted (Worthington et al, 2001). Because conduits can transmit groundwater much faster (up to several km per day) than the carbonate bedrock matrix, substantial aquifer heterogeneity exists as water moves much more slowly through the bedrock matrix relative to conduits (Kincaid and Werner, 2008, Brown et al., 2016). As cave networks evolve and become more complex, regional flow paths are altered (Figure 2) and travel time distributions in the aquifer become significantly more skewed (Dreybrodt et al., 1999, White, 2002, Ronayne et al., 2013). Thus, single ages typically reported by radiometric dating methods simplify timescales of karst aquifer recharge and subsequent discharge.

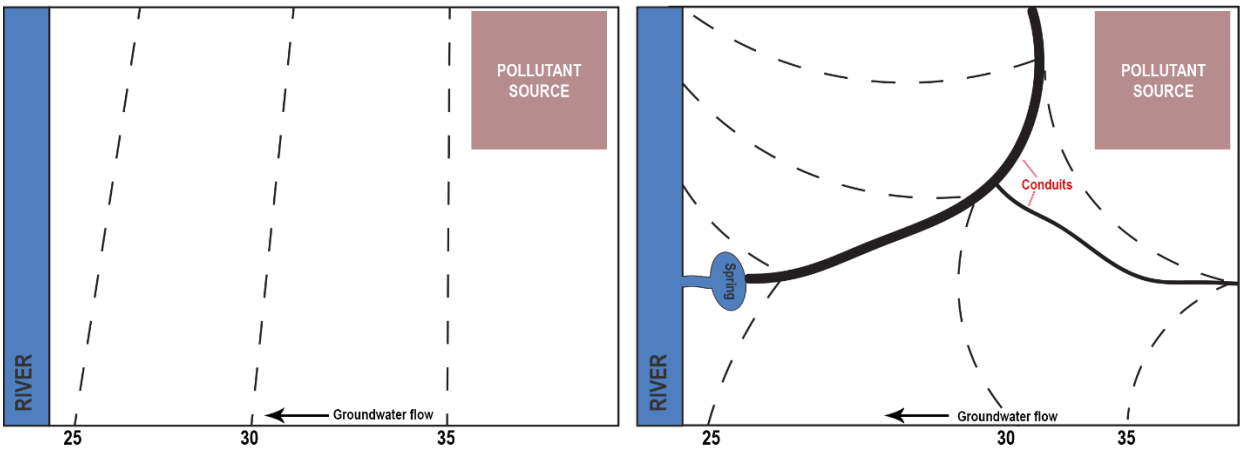

Figure 2: Hydraulic head gradient changes due to conduit development and adjustment to travel times. (Left) When a river boundary occurs and water levels grade toward the hydraulic low with no conduits. (Right) Illustration of when conduits intersect regional flow paths. When conduits intersect flow paths, the travel times decrease and pollutants can move much more quickly to a surface water body.

The FAS is even more complex than many classical karst aquifers, because lack of deep burial or porosity occlusion has resulted in retainment of depositional matrix porosity and substantial volumes of groundwater are recharged, stored, and transmitted through the fissured, fractured, and highly porous bedrock matrix (Budd and Vacher, 2002). This classifies the FAS as a triple porosity karst aquifer, and the resultant complex flow dynamics fundamentally impact water and solute transport. Further, the primary mechanism of cave formation is via diffuse recharge (Florea 2006), which creates a random patchwork of caves, some of which their locations are known while others remain undiscovered. The high matrix permeability integrates these porosity elements together, fundamentally controlling the storage and transmission of water and pollutants throughout the aquifer. The integration is substantial enough that dye tracing a

single surface point input have shown it is challenging to disentangle unique contributing groundwater zones of multiple first magnitude springs (Greenhalgh et al., 2016).

Implementing water resource management initiatives to improve the health of springs, rivers and lakes in the triple porosity FAS can be challenging. Groundwater that supports surface water ecosystems can be sourced from multiple areas of the landscape. When cave systems become more extensive and complex, waters can mix from wide ranging pollutant sources across the landscape and some sources may be more impactful than others. Furthermore, the transport and fate of pollutants would be impacted by the source such as when increased Biological Oxygen Demand (BOD) shifts redox conditions and affects nitrate concentrations. Additionally, it is widely understood that knowing the extent, morphology, integration, and location of phreatic conduits are necessary for accurate flow and solute transport simulations in karst aquifers (Scanlon et al., 2003, Kincaid et al., 2005, Shoemaker, 2009, Kuniansky, et al., 2016), as these factors are important for conduit flow, conduit and matrix exchange, and pollutant transformation and residence times. Because groundwater models are widely used for water resource management decisions, data collected can improve modeling efforts and their efficacy. Thus, state mandated initiatives such as Basin Action Management Plans (BMAPs) that aim to improve water quality by meeting Total Maximum Daily Loads (TMDLs) can be improved when unique sources of pollution are identified and conduit controls on flow and transport are understood which can lead to targeted actions taken to reduce loading.

Autonomous Underwater Vehicles (AUVs) can expand our knowledge of the subsurface by collecting high resolution water quality and physical data from karst conduits. Field data collection is a critical part of research that would ordinarily help answer many of the questions we have about aquifer dynamics. However, difficulty in collecting data from phreatic (fully saturated) caves has limited the information that goes into water resource decision making for spring water quality and quantity restoration efforts. Most water quality and survey data collection in caves have relied on certified SCUBA divers, but AUV's can explore regions of the FAS under conditions that certified divers cannot. AUV's can also be adapted to collect critical water quality and hydrological data that surface collection techniques are unable to acquire. With rapidly improving technology, AUV's are becoming a pivotal tool that can help answer pressing research questions that complement the objectives of water resource management.

This project is the initial effort to tailor the field-tested SUNFISH AUV to explore, map, and collect critical water quality and flow data in phreatic cave systems in Florida. Hereafter, we discuss the integration of a SeaBird Scientific Submersible Ultraviolet Nitrate Analyzer (SUNA) V2 on SUNFISH, improvement of current georeferencing capabilities, field deployment and testing

of these new features, and applying the already integrated technology onboard SUNFISH to generate a 3-D georeferenced cave map of Jackson Blue Spring.

SUNFISH AUV

Review of SUNFISH capabilities

SUNFISH (Figure 3) is a hovering AUV built by Sunfish, Inc. It is person-portable (50 kg in air), has a depth rating of 200 m, and is small and agile enough to maneuver in cave passages. This six-degree-of-freedom vehicle can assume any orientation and translate and rotate about any axis in any pose to precisely position and align its payloads. SUNFISH can be operated in three modes: (1) remotely, via a surface- or vehicle-deployed data fiber up to 2 km in length; (2) under supervised autonomy, where actions are autonomous but personnel at mission control can override; and (3) fully autonomously without fiber tether. The SUNFISH operational code base performs all of the basic functional tasks to allow for the mapping and navigation of caves and tunnels: station keeping; fixed stand-off maneuvering; obstacle avoidance; AUV health monitoring; data logging; 3D sonar mapping; dead-reckoning navigation; scripted mission capability; and supervised autonomy data link option. SUNFISH has been proven in numerous underwater cave sites both in the FAS and around the world (Ballard et al. 2020, Richmond et al. 2018, Richmond et al. 2020), moving through and producing 3D maps of these complex structures that scientific divers cannot always safely access (see Figure 4). Different sensors and equipment can be integrated onto SUNFISH to improve its utility for specific tasks. Examples of SUNFISH products, including from previous cave exploration and other sites can be found at https://sunfish.ai.

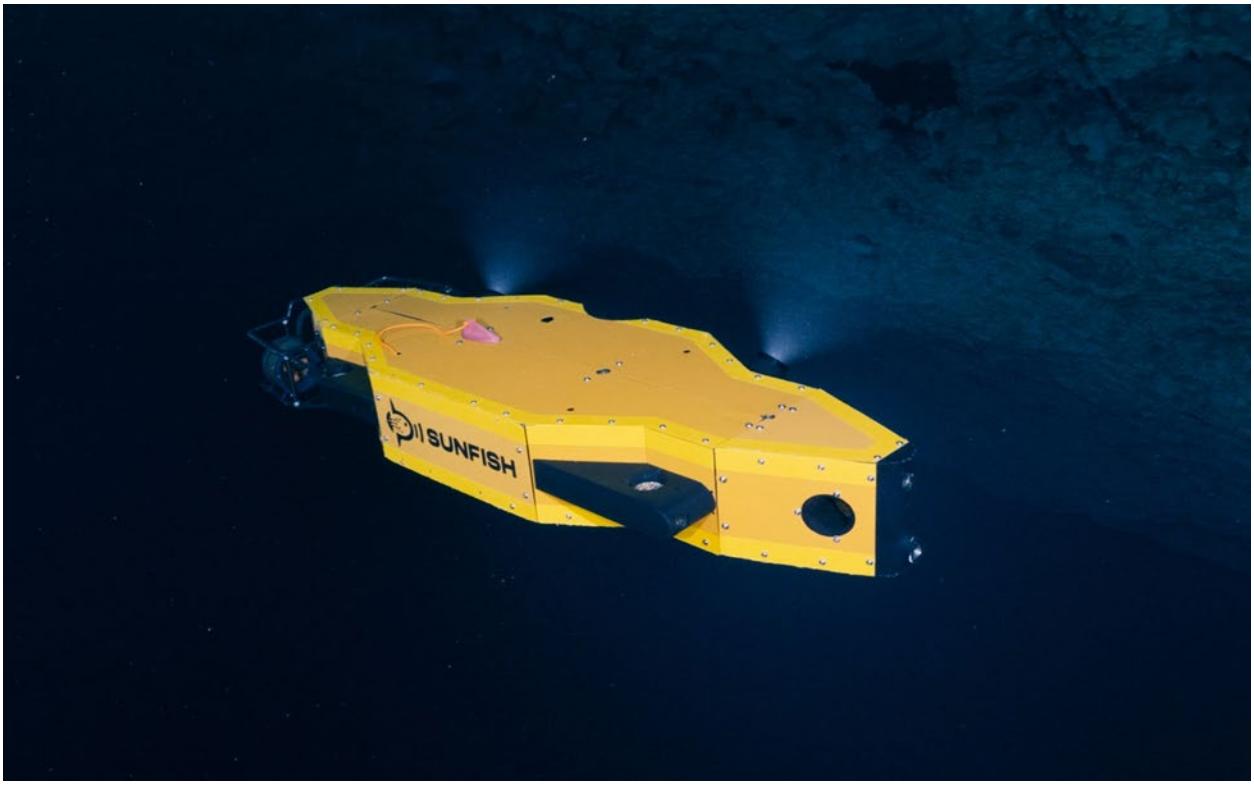

Figure 3. The SUNFISH AUV on a mapping mission in the Sally Ward Spring, FL

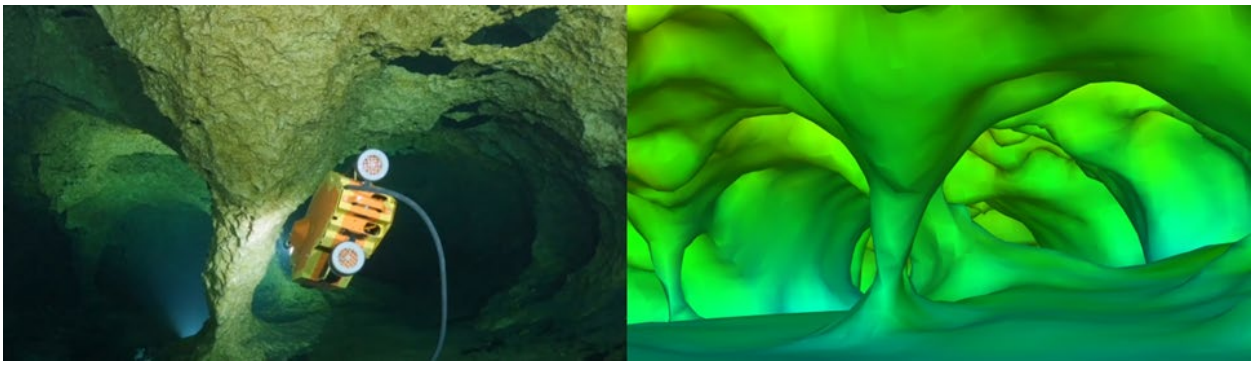

Figure 4. Views of the SUNFISH AUV exploring Peacock Springs, FL, and the resulting 3D map.

Table 3: SUNFISH specifications prior to upgrades for this project	

• Dimensions: 1.61 m x 0.47 m x 0.20 m
• Weight: 50 kg
• Depth Limit: 200 m
• Internal payload capacity:
  • *500 g wet weight*
  • *2.7 L (geometry restricted)*
• Speed: 1.0 m/s max, 0.4 m/s cruise
	• Sonar Mapping Operations:
	  • *Max ambient current: 0.1 m/s*
	  • *Minimum passage diameter: 2 m*
	  • *Resolution: 0.1 m*
	• Range:
	  • *Open water: 12 km*
	  • *Overhead environment: 1 km (tether limit)*
	• Navigation accuracy (under nominal conditions):
	  • *0.2 m relative to local map*
	  • *1% distance traveled relative to mapped features*

Table 4: List of base features on SUNFISH prior to upgrades and integration of new features

• Multibeam Sonar
  • *Large-scale, high-resolution cave maps: 10 cm combined resolution, maximum extent of 10s of km.*
• HD Imaging
  • *HD 1920x1080 imagery for general overview and close-up inspection of the cave.*
• Conductivity-Temperature sensor
  • *±0.02 mS/cm, ±0.05 ℃*
• Water depth sensor
  • *Depth accuracy: ±2 cm*

Site selection and description

Operations to test the integration of the SUNA nitrate sensor and map conduit geometry and extent were performed at Jackson Blue Spring in Marianna, FL. The site originally planned for the project was Wakulla Springs which is well mapped and contains surveyed wells and sinkholes which can act as control points for validating the georeferencing capability and water level gradients. However, during the project deployment window of April 15–May 17, 2024, flow conditions and visibility presented risks to divers and were not favorable for SUNFISH operation. Further, because forecasted weather conditions for the deployment window would continue to hinder operations at springs across Florida, only a few springs were accessible for this project due to brown outs from river reversals, flow, and overall cave accessibility. From existing maps of the Wakulla Springs operating area and previous experience operating in the cavern in 2023, we determined a maximum flow for operations in Wakulla Springs of a 24-hr maximum of 600 ft^3/s at the USGS monitoring station 02327022 (https://waterdata.usgs.gov/monitoring-location/02327022). While the historic median flows in the deployment window have been less than this limit, in the week just prior to the deployment window, flows at this station reached 24-hr maxima of 1800 ft^3/s with projected recovery times of several weeks. However, the primary determining factor in excluding Wakulla Springs as a site for this project year was that proposed operations required divers to escort the vehicle to obtain verification data using traditional collection methods with a YSI EXO^2 and manual discrete water sampling (see "**Validation of nitrate, conductivity, and temperature reading on SUNFISH**" below), and visibility in the cave was not expected to recover.

After conditions at Wakulla Springs were determined to be unworkable, USF, Sunfish, FGS, and DEP assessed 4 alternate deployment sites for field validation of the vehicle upgrades, and Jackson Blue Spring was suggested by the Florida Geological Survey (FGS) and FDEP as the primary backup. Though flow velocity and minimum diameter conditions in Jackson Blue Spring were expected to be outside the specifications for the SUNFISH vehicle to achieve high-resolution, full-accuracy mapping, the decision to deploy in this location for mapping was made in consultation with FGS and DEP to ensure that the field testing of the integrated systems which were the focus of the project could take place in the available project timeline. Additionally, diver support was available due to experienced divers familiar with Jackson Blue. The field operations are discussed more in detail under "**Summary of SUNFISH field operations."**

Jackson Blue Spring

Jackson Blue Spring is a karst spring located within the Dougherty Karst Plain. The Dougherty Karst Plain contains flat and irregular plains and has a characteristic karst topography that includes sinkholes, variably dry caves, and an evolved phreatic cave network that transmits groundwater through the aquifer. Jackson Blue is one of several explored phreatic caves within the region. Jackson Blue is one of several explored phreatic caves within the region. Using GIS of the springshed downloaded from the Florida DEP website (https://geodata.dep.state.fl.us/datasets/ab40667d9b844e0d91037fdbea0535aa/explore), the estimated groundwater contributing area to the spring is about 168 mi^2 (Figure 5). In the northern part of the spring basin, upper bedrock geology is primarily Ocala Limestone with some Eocene residuum, while the southern part of the spring basin contains Suwannee and Marianna Limestones which are situated above the Ocala Limestone; and together these units comprise the UFA (Figure 6). There exist regions of patchy aquifer confinement, but hydrogeologically, the UFA is unconfined, and depth to the UFA varies between 2-26 ft within the springshed area (Figure 7). The Marianna and Suwannee limestones are where phreatic caves such as Jackson Blue are contained and thus most caves are draining the vulnerable, unconfined UFA.

Jackson Blue Spring is a first magnitude spring with a discharge (Q) of > 100 cfs and is the primary source of flow to Merritt's Mill Pond. Merritt's Mill Pond is a 202-acre spring ($8.7x10^6$ ft^2) spring fed lake that serves as the headwaters to Spring Creek, whose waters eventually intersect the Apalachicola River (Dodson, 2013). Several identified springs provide flow to Merritt's Mill Pond, but Jackson Blue represents over 70% of the total contribution. Available discharge from the USGS Water Watch site for Jackson Blue Spring is shown in Figure 8. Though the measured discharge record is short (2001-2010), it spans several hydrological years. Analysis of the discharge data that was downloaded from the USGS Water Watch site resulted in a calculated average discharge of 158 cfs, and a maximum reported discharge of 490 cfs in April of 2005. More recent reporting has used these discharge measurements and nearby groundwater data to generate relationships that illustrate how groundwater level changes are highly correlated with changes in spring discharge. Recharge to the unconfined UFA sustains Jackson Blue discharge, which varies seasonally. The recharge rate to Jackson Blue Spring has been estimated to be between 12-18 in (304 – 457 mm) per year (Barrios, 2011).

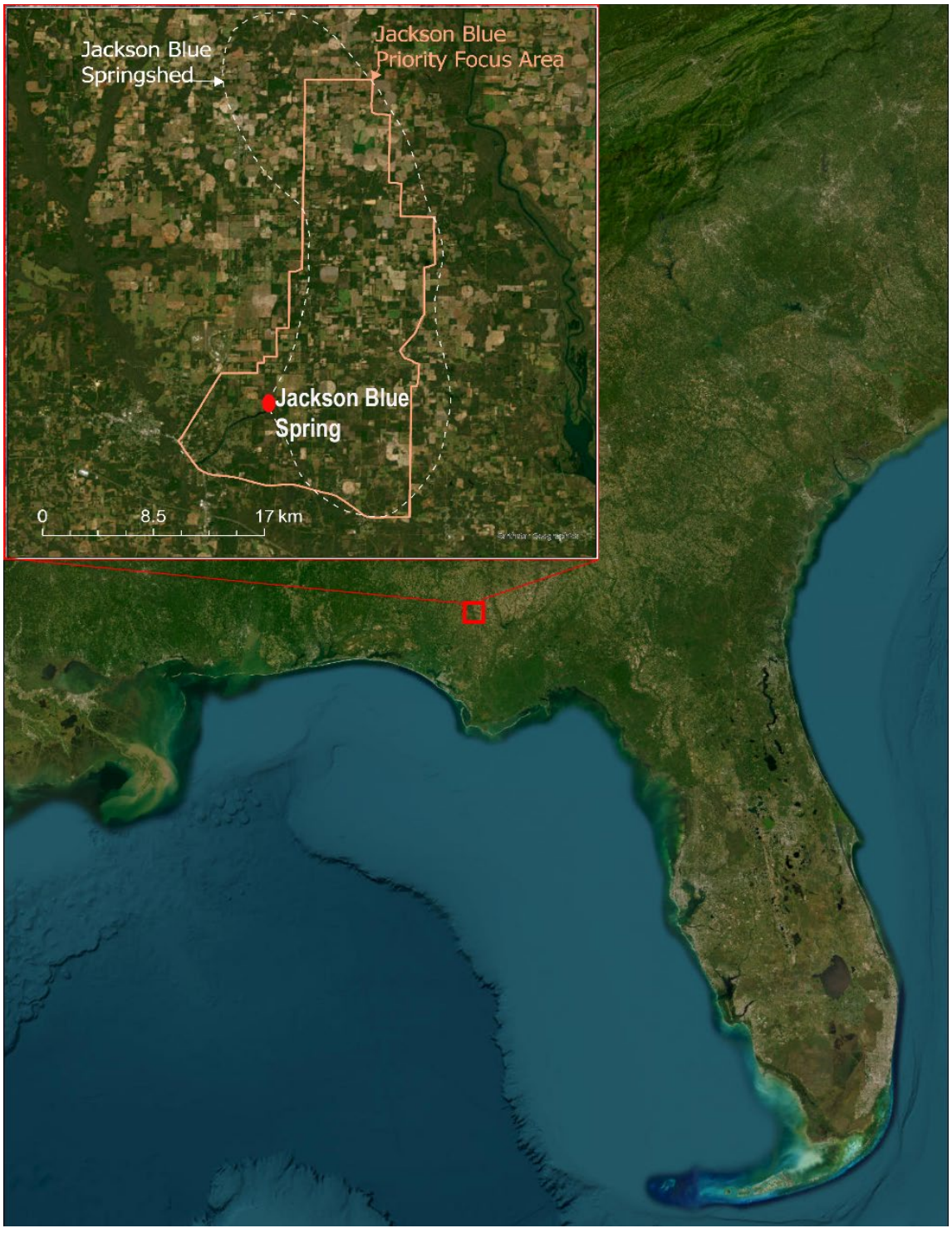

Figure 5: Location of Jackson Blue Spring area in the Dougherty Karst Plain and eastern panhandle. Both the springshed identified from topographic maps and later refined through potentiometric surface contours is shown as white dashed line. The priority spring area is shown as a solid orange line.

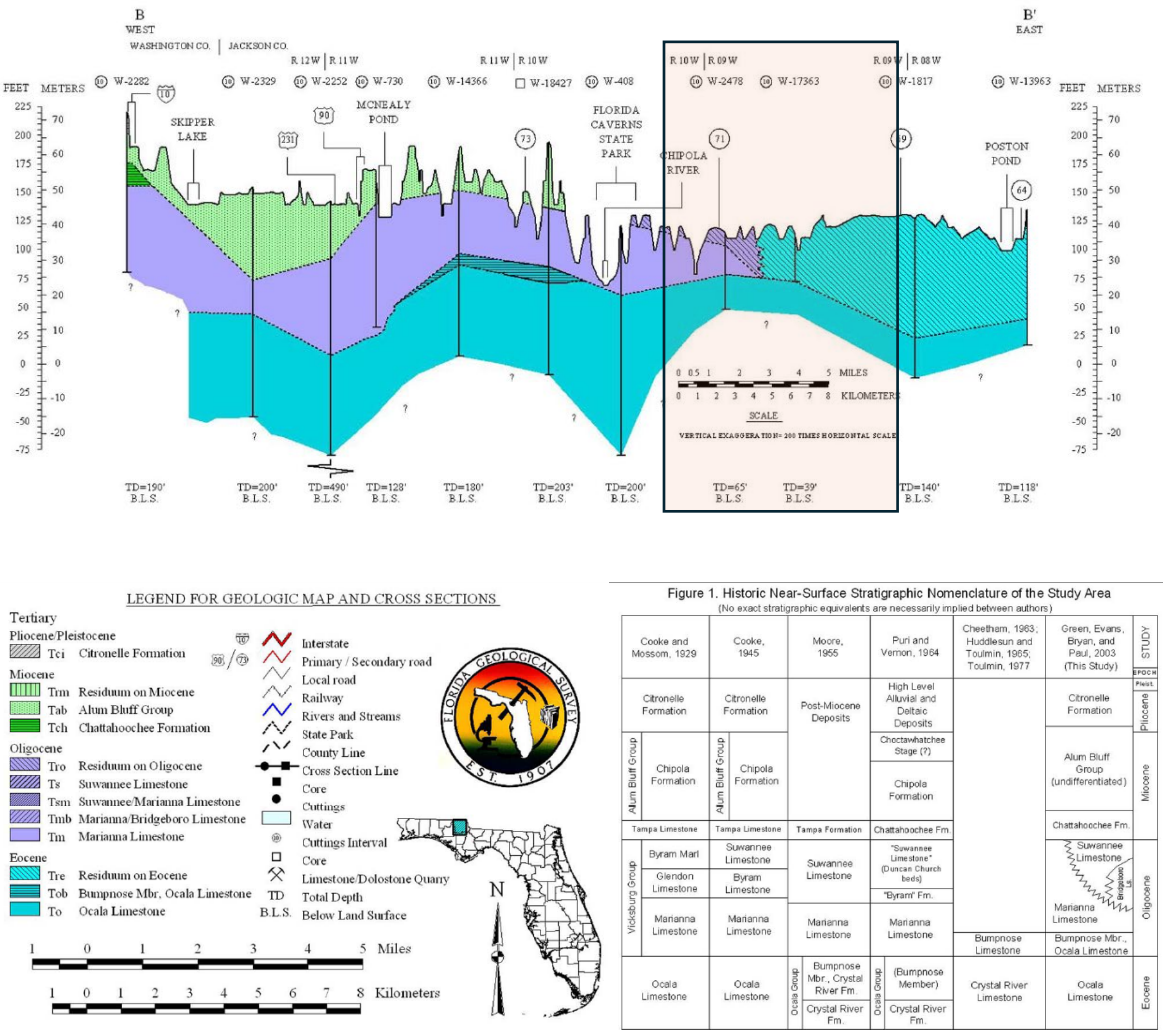

Figure 1. Historic Near-Surface Stratigraphic Nomenclature of the Study Area
(No exact stratigraphic equivalents are necessarily implied between authors)

Cooke and Mossom, 1929	Cooke, 1945	Moore, 1955	Puri and Vernon, 1964	Cheetham, 1963; Huddlesun and Toulmin, 1965; Toulmin, 1977	Green, Evans, Bryan, and Paul, 2003 (This Study)	STUDY
Citronelle Formation	Citronelle Formation	Post-Miocene Deposits	High Level Alluvial and Deltaic Deposits		Citronelle Formation	Pliocene / Pleist.
Alum Bluff Group: Chipola Formation	Alum Bluff Group: Chipola Formation		Choctawhatchee Stage (?)		Alum Bluff Group (undifferentiated)	Miocene
			Chipola Formation			
Tampa Limestone	Tampa Limestone	Tampa Formation	Chattahoochee Fm.		Chattahoochee Fm.	
Vicksburg Group: Byram Marl	Suwannee Limestone	Suwannee Limestone	"Suwannee Limestone" (Duncan Church beds)		Suwannee Limestone / Ocala Gp.	Oligocene
Glendon Limestone	Byram Limestone		"Byram" Fm.			
Marianna Limestone	Marianna Limestone	Marianna Limestone	Marianna Limestone		Marianna Limestone	
				Bumpnose Limestone	Bumpnose Mbr., Ocala Limestone	
Ocala Limestone	Ocala Limestone	Ocala Gp.: Bumpnose Mbr., Crystal River Fm.	Ocala Gp.: (Bumpnose Member)	Crystal River Limestone	Ocala Limestone	Eocene
		Crystal River Fm.	Crystal River Fm.			

Figure 6: Upper and Lower Floridan Aquifer in the vicinity of the Doughtery Karst Plain. Data obtained from FGS Dougherty Karst Plain geology - Green et al., 2003 – FGS Map Series no. 92.

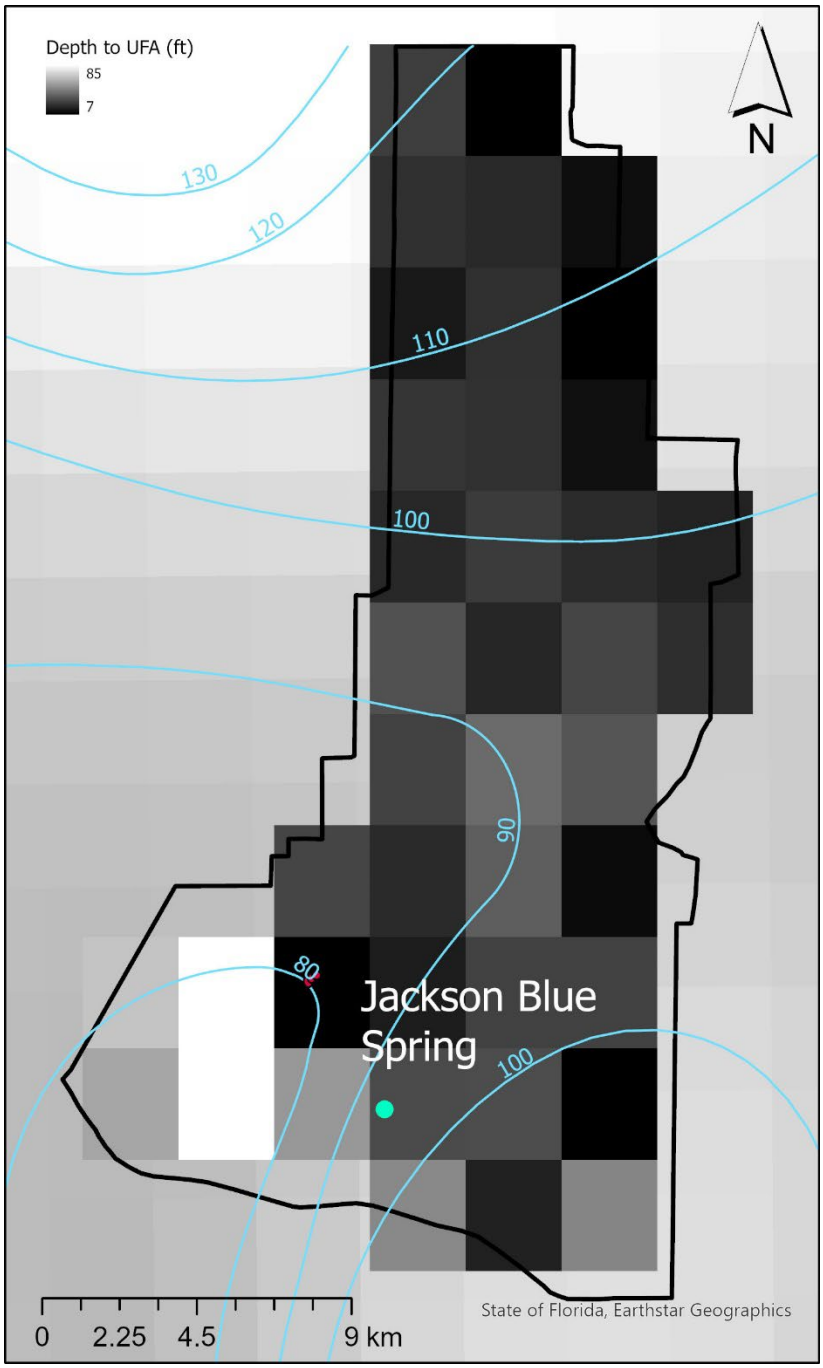

Figure 7: The depth to water level within the Spring Priority Focus Area (black outline). Potentiometric contours of the UFA are shown in blue and values are in feet. Values for the raster (black and white) were obtained by generating a water table raster from 2017 potentiometric contours and subtracting that raster from the land surface elevation DEM (see Figure 10). Some error appears to have occurred (white) around Merritt's Mill Pond.

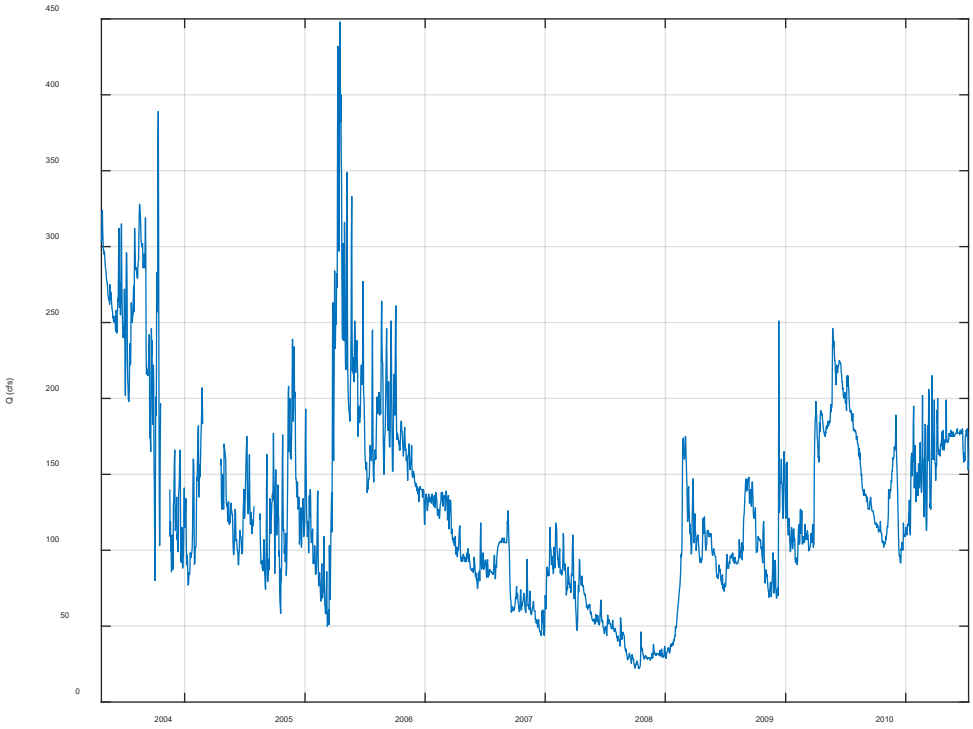

Figure 8: Jackson Blue Spring discharge from the USGS website. Green shaded areas on the bottom indicate approved data.

The Jackson Blue Spring basin contains substantial agricultural land use (Figure 9). Over the last several decades Jackson Blue Spring has shown increases in nitrate. A more thorough overview of water quality changes is provided in **Section IV: Merritt Mill Pond Sampling**. However, in summary, most of the water quality changes are related to agricultural land use contained within the spring basin based on isotope analysis conducted by Katz, 2004 and followed up with analyses from Barrios, 2011. Surficial sediments in the spring basin are primarily sand and with patches of sandy loam and some clays (Green et al., 2003 – FGS Map Series no. 92), which likely results in limited water retention and thus high nutrient leaching potential.

With the decrease in water quality and algae growth likely due to nitrate pollution, Jackson Blue Spring represented a good location to test SUNFISH and collect water quality and map the conduit location and geometry. The current cave map for Jackson Blue Spring is not complete, and the cave continues further (Figures 12-13). Further the cave map for the first section is only

available as a low-resolution stick map with limited information about the exact location, diameter, and continuous depth of the conduit.

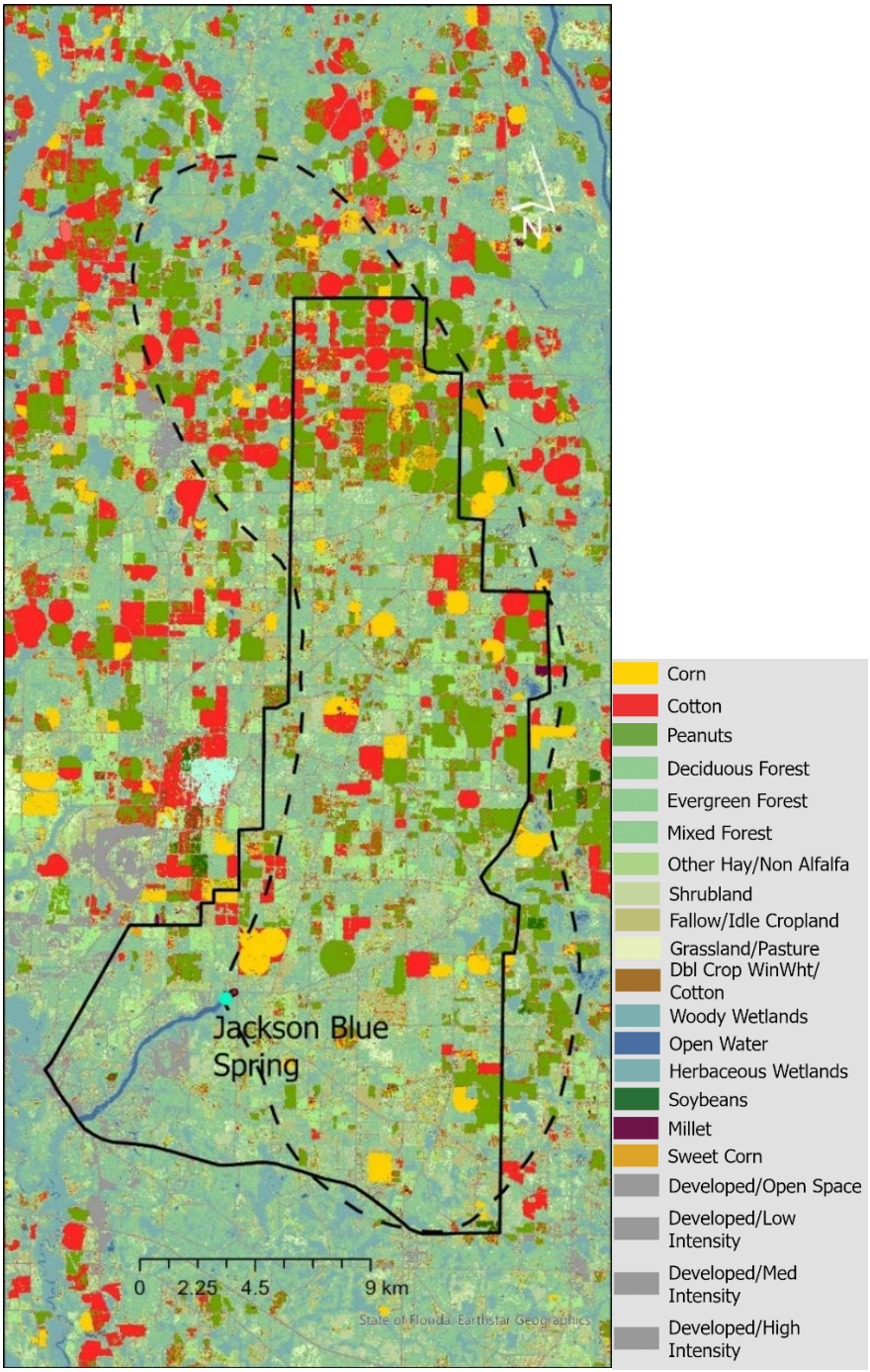

Figure 9: CropScape 2023 data for the Jackson Blue Springshed. Color coding for the most abundant crops within the Jackson Blue Springshed (Dotted Line). CropScape data retrieved from https://nassgeodata.gmu.edu/CropScape/. For the Jackson Blue Springshed - evergreen is the largest category and makes up 27%, and the remaining categories are: peanuts (18%), cotton (10%), fallow (10%), woody wetlands (7%), hay (7%), corn (5%), shrubland (5%), developed-total (4%), grassland (3%) with everything else <1%.

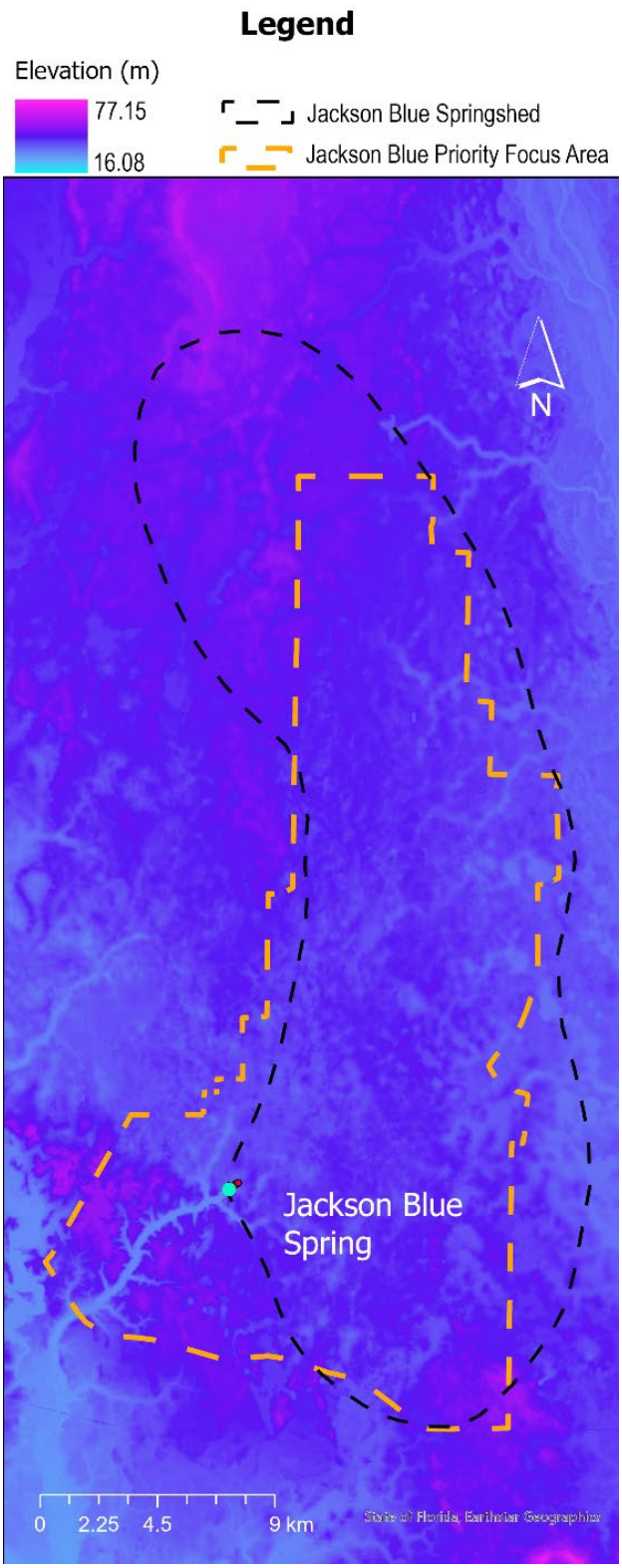

Figure 10: DEM that contains Hackson Blue Spring Priority Focus Area (orange dashed line) and springshed (black dashed line). DEM has a resolution of 30m and was obtained from The National Map Viewer run by the USGS.

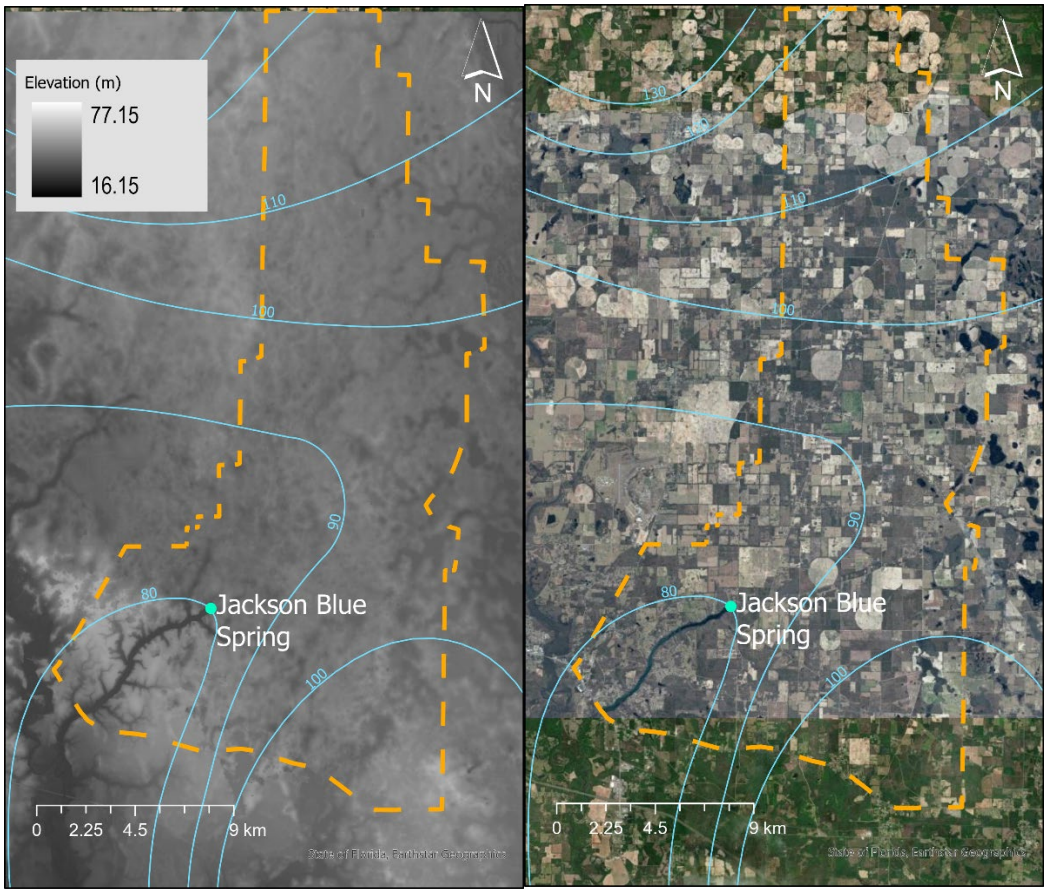

Figure 11: Potentiometric contours (feet) of the UFA shown within the Priority Focus Spring Area (orange outline) for Jackson Blue with DEM (left) and USGS Landsat satellite data provided in ArcMap Pro (right). Water level truncated to Priority Focus Area as the potentriometric surface does not include Georigia, but the springshed area does.

Figure 12: Current stick map of Jackson Blue Spring developed by cave divers with the National Speleological Society (NSS) Cave Diving Section (CDS) and provided by Cave Adventurers.

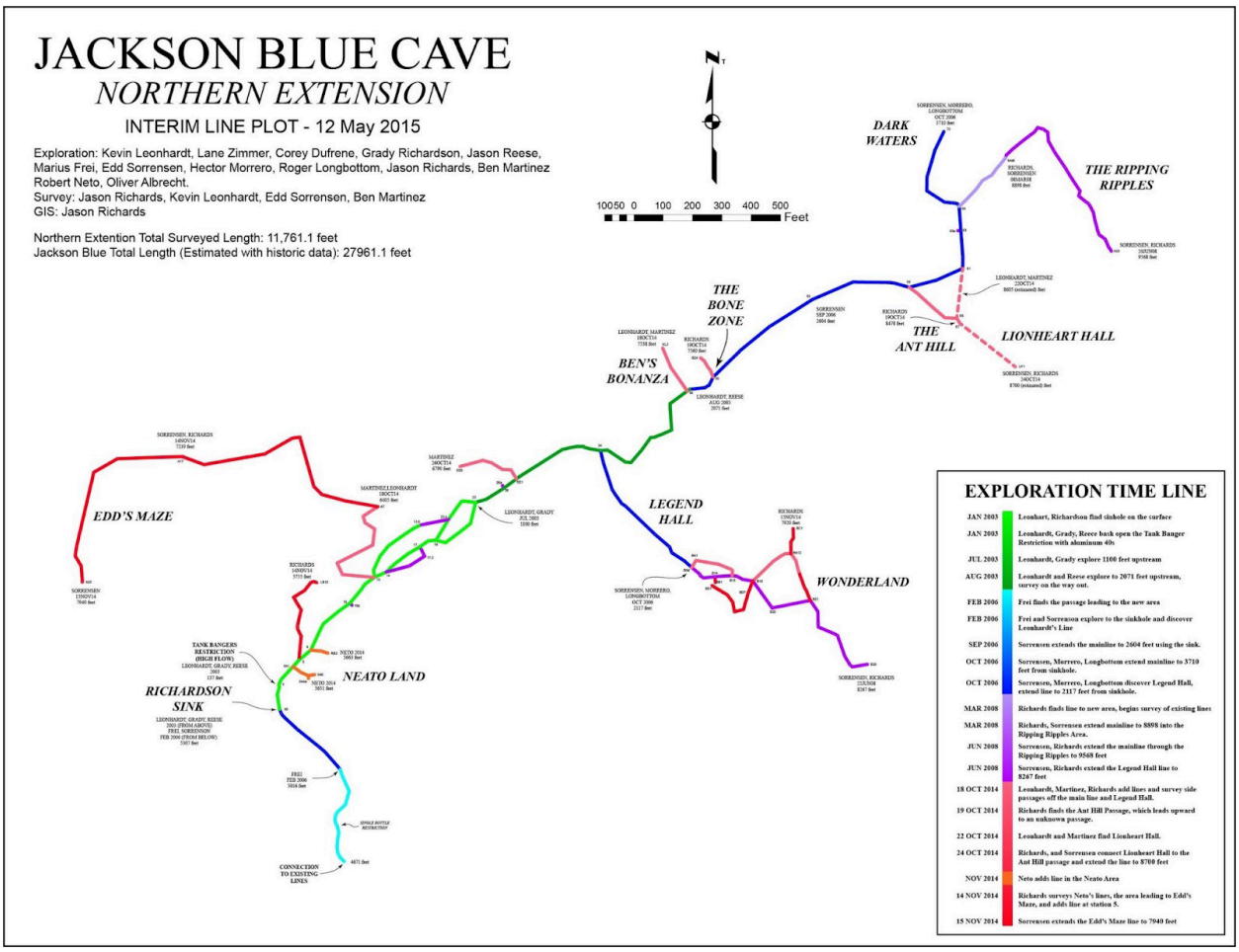

Figure 13: Extended, mapped passages of Jackson Blue Spring cave system. Map was downloaded from https://www.rchrds.org/florida_blog/2017/7/28/jackson-blue-cave and exploration and mapping were performed by divers mentioned in the image.

SUNFISH OPERATIONS

Nitrate sensor integration and testing

Sensor description and integration

The remote nitrate sensor selected was the SeaBird Scientific Submersible Ultraviolet Nitrate Analyzer (SUNA) V2 sensor. The nitrate analyzer, hereafter referred to as the SUNA sensor, is a portable spectrophotometer that uses the ultraviolet light spectrum at 254 and 350 nm to continuously sample nitrate in aquatic environments. There are multiple versions of the SUNA sensor that have variable features such as different pathlengths (5 mm, 10 mm), wider

depth ranges (100 m, 500 m) and factory calibration (freshwater, saltwater). We selected the freshwater, 100 m, 5 mm pathlength version for integration onto the SUNFISH AUV. The SUNA was selected out of several other nitrate sensors, and the comparison and reason for selection is described in APPENDIX B which was previously provided to DEP.

The nitrate integration plan was developed by SUNFISH and completed in late 2023. The full integration plan and schematics can be found in APPENDIX C, which was previously provided to DEP.

Field Operations - Conduit Mapping

Deployment of SUNFISH occurred from April 22nd to April 26th, 2024. Initial operations at the site on April 22nd and 23rd were aimed at vehicle set up and shakedown, assessing actual flow velocities and conduit sizes, and orienting the dive team to operations with the vehicle. SUNFISH was operated with a thin surface-fed fiber tether to supervise its operation in the face of known risks. Communications were received at a control station set up on the east shore of the spring (Figure 14), opposite and out of the way of the recreational diver entry area. It was found that flow velocities were too high in several sections of the first 100 m of the tunnel for standard SUNFISH mapping operations. Standard mapping involves oscillations along the vertical axis of the vehicle to scan the mapping sonar and achieve full, high-density coverage of the walls from multiple view angles. In the flow conditions encountered, the vehicle was unable to maintain standoff from tunnel walls during these mapping maneuvers, affecting both the mapping and navigational sensors. During these two days, the Sunfish team developed a field update to the vehicle software to allow for a modified behavior maintaining the vehicle nose pointed into the prevailing flow while rolling the mapping sonar, all under the guidance of a human operator (the “Gator Roll”). This enabled the vehicle to move through and map the tunnel at the cost of more human intervention and at significantly lower overall mapping data density, which also precluded navigational aiding from the vehicle Simultaneous Localization and Mapping (SLAM) system.

Figure 14: Location of the control station relative to the vent at Jackson Blue Spring.

The first full mapping deployment took place on April 24th. In order to enable further penetration while controlling the vehicle, SUNFISH was outfitted with a 680 m remnant disposable fiber spool, allowing the fiber to deploy from the vehicle and eliminate effects of tether friction or entanglement. This deployment was also used as the sensor validation run (see Validation section below). It was found that in some areas further from the entrance, where the conduit widened and flow velocity reduced, it was possible to perform high-density sonar scans. However, the scarcity

of such areas, and the tunnel height often near or below the 2 m limit still precluded standard mapping operations. A turn-around point of two-thirds of the available spool length (450 m distance from the shore where the fiber was connected) was agreed upon between the SUNFISH team, USF, and the dive team, relying on the presence of divers to disentangle fiber or recover the vehicle if available tether ran out (for unattended operations with the disposable fiber, standard turn-around is one-half of the spool length minus a constant length that depends on precise spool geometry). SUNFISH turned around after 446 m, but had difficulty holding standoff position in the flow now coming from its stern. It was decided the safest course of action was to allow the accompanying divers to recover the vehicle and disposable fiber. The divers manually reeled in the fiber during the return, and it was disposed of upon recovery. Despite the challenges presented by the flow and narrower passages, on this run, SUNFISH was able to provide the data for a 3D georeferenced map with co-located nitrate, conductivity, and temperature.

On April 25th, the available dive team was reduced, so the team focused on engineering tests of behaviors for moving and mapping with a following flow, other automated behaviors to attempt to automate mapping under the conditions experienced in Jackson Blue—including deeper integration of the Gator Roll maneuver into the vehicle software—and higher-density scans of the upper section of conduit near the entrance where possible.

On the final deployment day, April 26th, with the lessons learned from the previous days, SUNFISH performed a second mapping run with a 2 km disposable fiber. Based on recommendations from the dive team that the conduit height shrinks not far beyond the turn-around point from April 24th, turn-around was to be determined by accompanying divers' limits. The vehicle achieved furthest penetration of 440 m of fiber (420 m from the entrance) for this deployment. The vehicle was able to return under its own control for 130 m, but in the face of more difficult control in the following flow, and several extended navigation outages due to the failure to maintain standoff, the dive team ultimately was called upon to recover the vehicle and the disposable fiber that had been spooled out. Data from this run provide an additional measure of the confidence in the 3D map of the conduit. While a direct comparison with the April 24th mapping run is made difficult by the number of navigation outages and low mapping data density imposed by the Jackson Blue environment, efforts to derive a lower bound on georeferenced map confidence will continue in the enhancement period.

Calculation of conduit map uncertainty

Spatial Dataset

At the time of this report, the spatial data set has a single Global Navigation Satellite System (GNSS) Real Time Kinematic (RTK) positioning fix taken at the surface of Jackson Blue Spring to aid in positioning the survey. Relying on a single GNSS fix, however, results in significant positional errors due to the inherent inaccuracies of an AUV's navigational system, which drifts over time once the vehicle is submerged. This inherent drift was particularly exacerbated for SUNFISH by the conditions and conduit size at Jackson Blue Spring which both degraded performance of the Doppler Velocity Log (DVL) navigation sensor and precluded navigation corrections based on mapping data. One method to improve the positional accuracy of the survey is to take multiple GNSS fixes throughout the mapped conduit to aid the navigational system. To achieve this at Jackson Blue Spring, a second survey performed by divers is underway to establish control points throughout the cave, using traditional cave survey radiolocation methods to obtain GNSS fixes. These control points will be used to reprocess the survey data and achieve higher positional accuracy .

The following accuracy analysis applies to a spatial dataset with a single GNSS fix that is not validated by an independent higher-accuracy source. . The dataset is being reported as a composite dataset with varying accuracies. The following reports the accuracy value for the least accurate dataset component.

Compiled to meet

- 80 meters horizontal accuracy at 95% confidence level
- 2 meters vertical accuracy at 95% confidence level

Both horizontal and vertical positional accuracy were derived from first principles using guidance in references (ASPRS 2023, Hegrenaes et al. 2010, Jalving et al. 1999). The ASPRS 2023 Positional Accuracy Standards were used as a guide, although the scope of that standard is data produced from aerial photographs, satellite imagery, and ground surveys—not underwater sonar with dead-reckoned navigation. To obtain positional accuracy for this survey, the following error analysis was conducted looking at each isolated error source and then propagating the uncertainties. Analysis was conducted using estimated standard deviations (1σ) and then converting the result to 95% confidence levels assuming a normal distribution of errors.

Trajectory Accuracy

All mapping data are tied to the vehicle trajectory (position and orientation over time). This in turn has two components: the horizontal position which drifts with time, and the vertical position, which is always referenced to the surface pressure assuming hydrostatic equilibrium

Horizontal Trajectory Accuracy

To determine the theoretical best accuracy, the following assumptions were made:

- Starting position error is 0.2 m based on the upper bound of the Advanced Navigation Poseidon RTK-GNSS antenna
- Starting heading error is 0.95° based on tested alignment errors demonstrated with ground control data.
- Tilt error is 0.01° based on the Advanced Navigation Fiber Optic Gyro (FOG) Inertial Navigation System (INS) specified error
- Doppler Velocity Log (DVL) drift versus time is 0.2 cm/s based on the manufacturer's specifications
- DVL drift versus distance traveled is 0.4% based on the manufacturer specification
- DVL outages occur when less than 3 beams are providing velocity estimates
- Max penetration distance was 420m
- DVL position drift vs outage time is defined by Equation 1.

$$\Delta p = sin(\theta_e) g t^2 \qquad \text{Equation 1}$$

Where Δp is position drift, θe is minimum tilt error, g is acceleration due to gravity, and t is outage duration.

For Jackson Blue Spring underwater surveys where there is a dearth of control points and satellite positioning at the water surface, and thus the positional accuracy deteriorates as a function of survey time and distance from a surface fix. As shown in Figure 15, the horizontal Root Mean Squared Error (RMSE) increased with survey duration; positional accuracy is worst at the furthest penetration of the survey. The various contributions to total horizontal RMSE at the point of furthest penetration is shown in Figure 16. Most errors accumulate from the Doppler Velocity Log (DVL) sensor which forms the basis of the dead-reckoned navigation solution. The "DVL Time" term is a direct function of the duration of the survey and hence the speed at which the vehicle can move while navigating the tunnel. The "DVL Outage" term is attributable to loss in the DVL sensor signal during the survey, mostly due to violating the sensor's minimum range in narrow constrictions or areas where the vehicle is unable to consistently hold standoff in high flow. Figure 17 shows the durations of individual DVL outages during the survey.

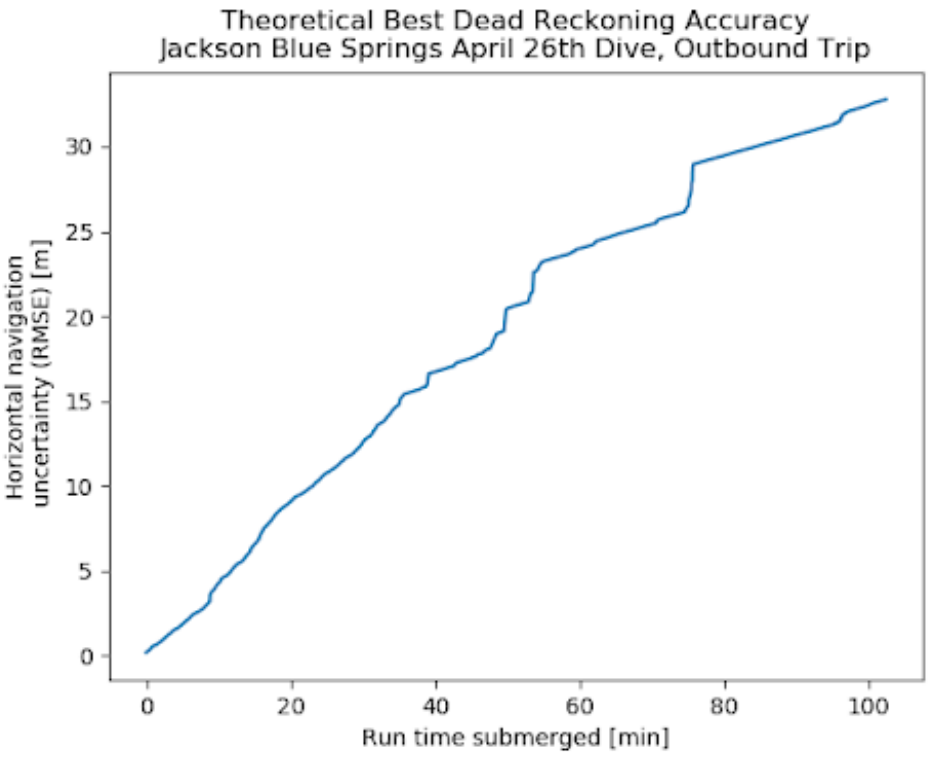

Figure 15: Horizontal RMSE as a function of distance from the surface position fix at the entrance.

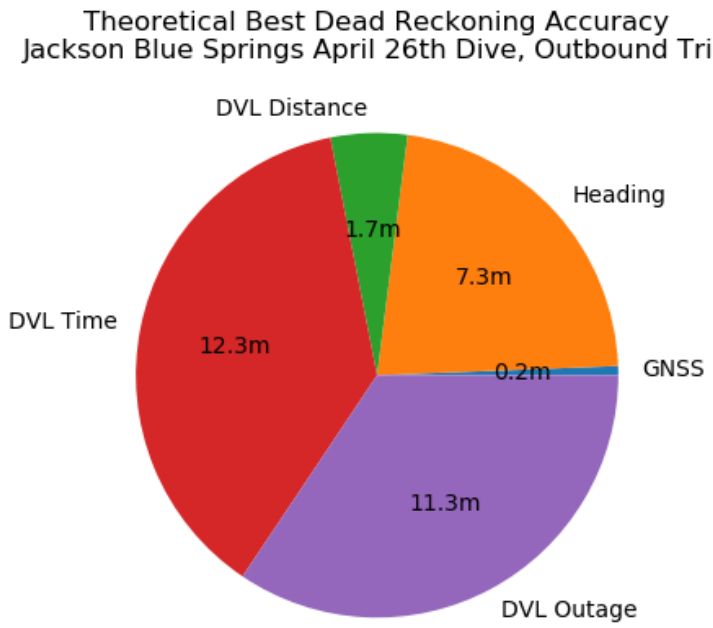

Figure 16: Individual RMSE horizontal accuracy sources at the furthest point of survey from the surface position fix at the entrance.

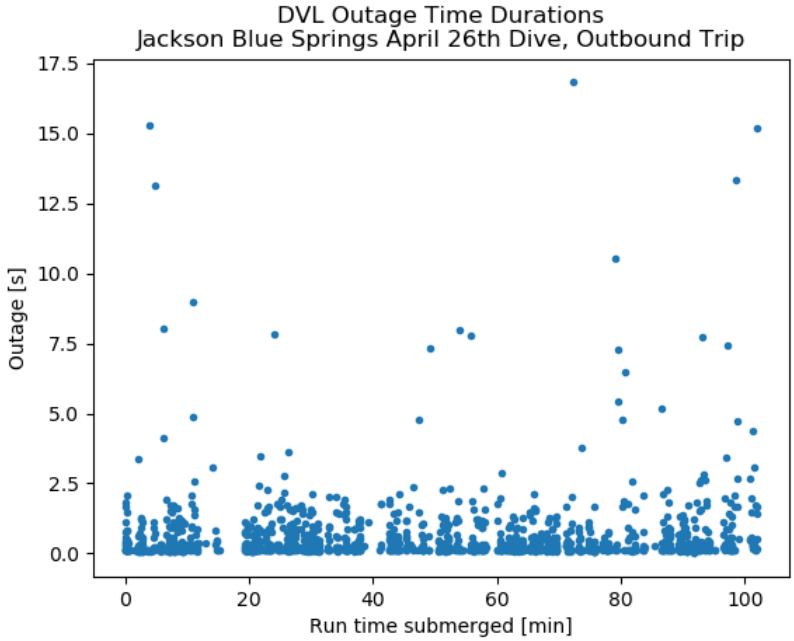

Figure 17: Time and quantity of DVL outages during the survey. Outages longer than 5 s significantly affect the navigation error, though total error grows the accumulation of all outages.

Vertical Trajectory Accuracy

The following assumptions were made to estimate vertical accuracy:

- Pressure sensor accuracy is 0.01% full scale based on manufacturers specifications
- Pressure sensor full scale is 200 m depth based on manufacturers specifications

The RTK-GNSS elevation estimate at the rover GNSS receiver should achieve highest accuracy after the vehicle has been stationary at the surface for a time that is dependent on environmental interference (i.e. trees or other sources of GNSS signal degradation). One operationally feasible method of minimizing error in a GNSS datum at the start of a mission is for the operator to monitor GNSS covariance and qualitatively select a time where initial high covariance has decreased and converged to a stable value, then to zero the local mission coordinates and pressure sensor. To reflect this process in postprocessing, the data logs were reviewed and a pre-dive GNSS altitude covariance value was qualitatively selected that reflected a nominal stable value. This analysis, shown in Figure 18, produced a GNSS RTK elevation accuracy of 0.95 m. Taking the geometric average of 25 measurements the elevation GNSS accuracy is $0.95 / \sqrt{(25)} = 0.19m$, 1σ.

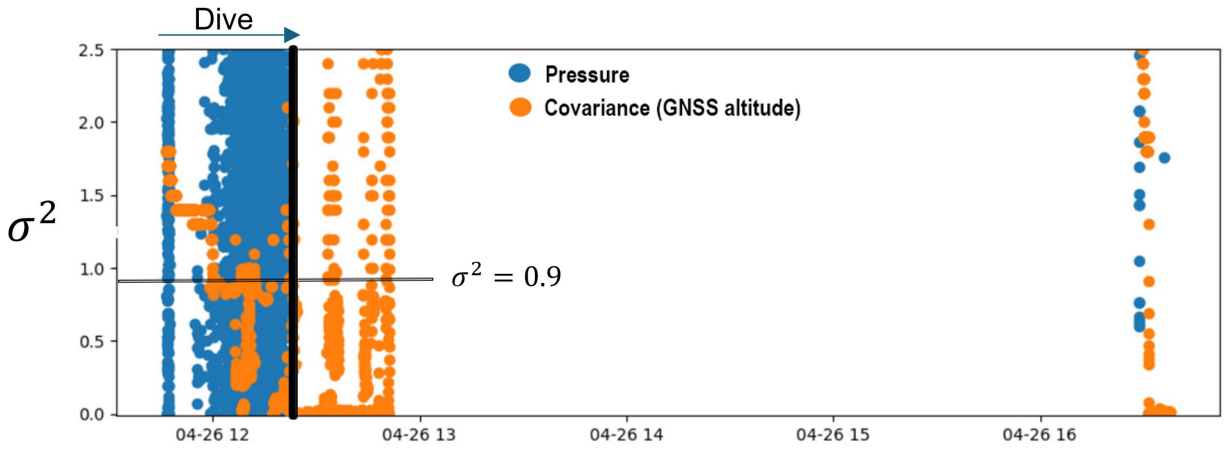

Figure 18: Pressure (Blue) and GNSS altitude covariance (Orange) for mission duration, vehicle submergence and "stable" surface σ^2 value annotated.

Map Accuracy

Once trajectory accuracy is estimated we can calculate the total propagated error for each multibeam sonar hit point or voxel in the map. For this analysis we make the following assumptions:

- Multibeam sonar max range is 20 m
- Multibeam sonar resolution is 1/500 max range based on multibeam DeltaT 837B specification (Where DeltaT is model name of sensor)
- Multibeam sonar transmit beamwidth is 3° along-track based on multibeam DeltaT 837B specification
- Multibeam sonar receive beamwidth is 0.75° across-track based on DeltaT 837B specification
- INS heading error is 1° based on tested alignment errors demonstrated with ground control data.
- INS tilt error is 0.01° based on Advanced Navigation FOG INS specification
- Mounting roll uncertainty is 2° based on engineering estimate
- Sound speed is 1500 m/s in water
- Sound speed error is 0.25 m/s, 1σ based on (Jalving et al. 1999)

The following error sources are also considered:

- Sensor range resolution
- Beam pointing angle inaccuracy due to an erroneous sound speed value
- Beam range inaccuracy due to erroneous sound speed value
- INS orientation estimation errors
- Sensor versus INS orientation offset errors
- Along-track hit position uncertainty
- Across-track hit position uncertainty

The following errors were considered negligible:

- Multibeam range estimation error
- Multibeam penetration into the cave floor
- Multibeam refraction (beam bending) errors
- Sensor versus. INS latency errors
- Sensor versus INS position offset errors

The steps of the error propagation analysis are as follows:

1. Sensor range resolution

$$For\ this\ case, r = \frac{20\ m}{500} = 0.04\ m$$

2. Sound speed error will cause the estimated beam pointing angle to be erroneous:

$$sin^{-1}(\sin(\theta)\frac{\Delta c}{c})$$

Where:
$\theta = Beam\ incidence\ angle$
$c = Speed\ of\ sound$

For this case $< 0.01°, 1\sigma$

3. Speed of sound (c) error will cause the beam range to be erroneous:

$$\Delta r = r\frac{\Delta c}{c} \qquad For\ this\ case, \Delta r = 0.003\ at\ 1\sigma$$

4. INS orientation estimation errors:

   $For\ this\ case\ \Delta\theta = 0.01°$

5. Sensor versus INS orientation offset errors

   $For\ this\ case\ \Delta\theta = 2°$

6. Along-track hit position uncertainty

   Beamwidth is a Full width at half maximum which is the same as 2.355σ

$$\Delta x = r * \sin\left(\frac{BW}{2.355}\right)$$

   For transmit beamwidth of 3° along-track $\Delta x = 0.445m, 1\sigma$

7. Across-track hit position uncertainty

   For receive beamwidth of 0.75° across-track $\Delta x = 0.111m, 1\sigma$

Further:

- Angular error $\Delta\theta$ can be converted to range error $\Delta r = r\left(\frac{\cos(\theta)}{\cos(\theta+\Delta\theta)} - 1\right)$
- Range error Δr can be converted to perpendicular surface error $\Delta z = \Delta r\ cos(\theta)$
- Range error Δr can be converted to tangential surface error $\Delta x = \Delta r\ sin(\theta)$

	Total Accuracy, 1σ [m], r=20m				
Index	=0	=15	=30	=45	=60
1	0.040	0.040	0.040	0.040	0.040
2	0	0	0	0	0
3	0.003	0.003	0.003	0.003	0.003
4	0	0	0	0	0
5	0.001	0.010	0.021	0.037	0.065
6	0.445	0.461	0.514	0.629	0.890
7	0.111	0.115	0.128	0.157	0.222
Total	0.460	0.477	0.532	0.651	0.920

Table 5 : Table of ranges and accuracy r vs. beam incidence angle, θ .

Total accuracy is determined to be the geometric mean of these individual contributions: 0.59 m. The beamwidth contributes significantly to angular ambiguity. As a result, the sum of the dead-reckoned navigation error and sonar error constitutes the map error.

The total vertical error is estimated to be 0.8 m, 1σ using the geometric mean of:

- GNSS (0.19 m, 1σ)
- pressure (0.02 m, 1σ)
- multibeam (0.59 m, 1σ)

Validation of nitrate, conductivity, and temperature reading on SUNFISH

Nitrate

Validation of nitrate took place on the first full mapping deployment on April 24th, 2024. Discrete water samples were collected to confirm the nitrate readings on the SUNA sensor and quantify any parameters that could cause interference. Because the SUNA sensor uses spectrophotometric methods set at specified absorbance wavelengths (254 and 350 nm), interferences from other constituents that impact absorbance or have a peak absorbance at the same wavelength measured by the SUNA need to be considered. Parameters that could interfere with measurements include color, turbidity, and Dissolved Organic Carbon (DOC).

Discrete water samples were collected by cave divers at 3 sites inside the cave and from the Jackson Blue Spring vent and followed all protocol outlined in the QAPP. For sites sampled

in the cave, cave divers sampled water using syringes that had been filled with DI water and were extruded when sampling commenced. A sample was collected in a pre-labeled syringe and placed in a dive pouch for the remainder of the dive. Divers also carried a calibrated YSI EXO^2 continuously (Δt = 15 s) collecting pH, dissolved oxygen (DO), specific conductance, and temperature in the cave system. A video of divers collecting water samples was recorded by the SUNFISH vehicle and is provided to the DEP (Supplemental Data). Once divers emerged from the cave after the dive, syringes were immediately collected and used to fill pre-labeled sample bottles using the appropriate filters and preservatives. No problems were reported by divers during sampling. The vent was sampled using surface water sampling procedures and a pump to collect water. Several factors went into this decision including the additional sampling of other analytes (Table 6) and minimizing diver load on a support dive for SUNFISH. We used a Tornado plastic well pump because it was easier to weigh down in the flow and was a bright blue color so divers, including those not supporting SUNFISH, could see it while they were entering and exiting the cave. All DEP SOP protocol was followed for sample collection including ensuring tubing was free of contamination, purging the tubing prior to sampling, and sampling each analyte in appropriate containers (Table 6) and with appropriate filters. We note the preserved NO_x-N sample collection was done by USF and analyzed at cost to them.

Analyte (or group)	Vial	Filter	Analysis location	Chemical Preservative
Color	40 mL amber glass	0.45 micron	AEL	None
DOC	40 mL amber glass	0.45 micron	AEL	HCl
Turbidity	3x 20 mL plastic	None	AEL	None
Nitrate+Nitrite (NO_x-N)	2x 20 mL plastic	None	USF	H_2SO_4 (28-day hold)
Nitrate (NO_3^-)	20 mL plastic	None	AEL	None (48-hour hold)

Table 6: Analytes sampled in the cave and at the vent

All samples were immediately preserved on ice and transported according to protocol. The samples for color, turbidity, DOC, and NO_3-N (unpreserved) were immediately taken to Advanced Environmental Laboratories (AEL) in Tallahassee, FL. Analyses were performed within 48 hours for NO_3-N (unpreserved), turbidity, and color; DOC was analyzed within 14 days (APPENDIX C). The NO_x-N samples preserved using sulfuric acid were analyzed within 28 days at USF's water quality lab.

Conductivity and temperature

SUNFISH integrated C/T sensor validation also took place on April 24th, 2024. Onboard the SUNFISH AUV is an Neil Brown Ocean Sensor Incorporated (NBOSI) 100-series conductivity and temperature (C/T) sensor (www.nbosi.com) (APPENDIX D). To confirm the NBOSI conductivity sensor was accurately reporting data, we used 2 external conductivity sensors for validation during deployment. The 2 external conductivity sensors were a vanEssen conductivity, temperature, and depth (CTD) sensor and a C/T probe on a YSI EXO^2. The vanEssen CTD was mounted on SUNFISH while the YSI EXO^2 was carried by cave divers while they supported SUNFISH during deployment. The NBOSI C/T, vanEssen CTD, and YSI EXO^2 recorded measurements every 15 seconds.

The C/T onboard SUNFISH is fully integrated, and therefore traditional calibration of the C/T occurs in the lab prior to deployment. SUNFISH sent the C/T out to NBOSI for calibration prior to and following site deployment in 2024. Temperature on the NBOSI C/T was validated against a NIST thermometer standard prior to deployment (APPENDIX D). However, field validation using external conductivity sensors was also performed in case of 1) drift, which would require a bias correction of the recorded data or 2) malfunction because of SUNA sensor integration.

YSI EXO^2 and vanEssen conductivity and temperature calibration and validation

The YSI was calibrated on the morning of April 24th, 2024 while the vanEssen CTD conductivity was validated using known conductivity standards (84 and 1000 µS/cm) on 4/23/2024. The parameter values from the calibration of the YSI EXO^2 are shown in Table 7 while the readings for the vanEssen are shown in Table 8. The readings on the vanEssen were within 5% of the standard value indicating the sensor was functioning properly.

Parameter	Standard	Pre-	Post
pH (2-point)			
7.00	7.00	6.77	7.00
10.0	10.00	9.81	10.00
Conductivity	84 µS/cm	83.3 µS/cm	83.9 µS/cm
DO (%)	Air-saturated (100%)	98.2%	100%
Temperature	NIST – 25.2°C	--	24.99°C

Table 7: YSI EXO^2 calibration on the morning of 4/24/2024

Parameter	Standard	Reading	Difference
Conductivity	1000 µS/cm	980 µS/cm	2%
Temperature	NIST – 25.2°C	25.5°C	1.12%

Table 8: vanEssen readings of conductivity and calculated percent difference between measured value and standard. The reading represents the average values once the temperature had stabilized.

The vanEssen and YSI EXO^2 temperatures were validated against a USF lab National Institute of Science and Technology (NIST) thermometer. The temperature reported by the NIST thermometer was 25.2°C, while the temperature reading on the YSI EXO^2 was 24.99°C (0.8% difference) and the vanEssen conductivity sensor was 25.5°C (1.12% difference).

Results and Discussion

Conduit Mapping

The 3-D conduit data in .las format, georeferenced nitrate, time-synced temperature and conductivity data, and vehicle trajectory have been provided as deliverables to the DEP. Figures 19-21 show the cave map overlain on satellite imagery (Figure 19), a 30m Digital Elevation Model (DEM) topographic raster (Figure 20), and a CropScape 2023 cropland data map (Figure 21). The conduit polyline was created by using the coordinates provided in the georeferenced nitrate deliverable Excel sheet (Supplemental). The shaded error bounds were determined using a linear relationship ($y = mx + b$) (Figure 15) between the initial error (0.8 m) and the final error (32.8 m). The slope (m) of the line was determined by the difference in error between final penetration limit and initial error across the distance mapped (420 m). An intercept of b = 0.8 m assuming initial distance x = 0. This produced a relationship between distance (x) and the error (y). The polyline for the conduit was divided into equal segments (~0.8 m) and for the accumulated distance at the end of each segment, the error was calculated. Finally, a visual buffer around each segment was generated to produce the shaded error region. Additionally, the approximate locations where discrete water samples were collected to validate SUNA nitrate are shown in Figure 19 and the results are discussed in the following sections.

The goal for this initial pilot project was to demonstrate newly integrated sensing systems and the ability to georeference measurements with quantifiable error estimates. Some limitations at Jackson Blue made operations challenging for the current version of the SUNFISH vehicle, whose specifications are better adapted to the size and generally lower flow velocities in the Wakulla Springs main conduits. The flow at Jackson Blue Spring was exceptionally high after a series of rainstorms had occurred. Velocity measurements taken using an acoustic doppler current profiler (ADCP) in the spring vent ranged from 0.18-0.28 m/s, exceeding the 0.1 m/s limit for standard SUNFISH mapping operations which rely on rotating the mapping sonar sensor fore and aft to ensure along-track navigation updates. In addition, some conduit sections at Jackson Blue Spring are at or below the 2 m lower limit on tunnel diameter limit to allow for uninterrupted operation of the SUNFISH primary dead-reckoned navigation sensor. Finally, unlike other springs in Florida such as Wakulla Springs, the Jackson Blue cave system has no wells, sinkhole, or karst window control points, limiting validation of the maps produced by the vehicle. During the deployment, the USF and Sunfish team developed mitigation techniques to allow for continued operation and basic validation of the new vehicle capabilities (nitrate sensing and georeferencing)

that were the focus of this project. However, vehicle navigation and map quality were affected by the out-of-standard operations.

As a result of field conditions and adjustments, high-resolution mapping and high-accuracy georeferencing were made difficult. The newly developed “Gator Roll” could not address periodic navigation sensor outages due to standoff violations in areas where the tunnel headroom fell below minimum diameter, nor provide along-track navigation corrections from map data. For the processing of out-of-spec mapping data into a complete map, a rapid development of enhancements to the Sunfish processing software was completed before the end of the fiscal year, incorporating feedback from the DEP to ensure data products from the Sunfish processing could be ingested into DEP GIS systems. As a result, a complete, 3-D, georeferenced conduit map of Jackson Blue cave system was generated for the first ~420 m (1450’) of the cave with known georeferencing accuracy. Operations in environments compatible with current SUNFISH vehicle specifications, or additional enhancement of the vehicle capabilities will significantly reduce this maximum error.

Figure 19: The mapped conduit (red line) and horizontal error (shaded pink) associated with increasing penetration.

Figure 20: DEM and mapped conduit (red line) and horizontal error (shaded pink) associated with increasing penetration. The DEM was obtained from USGS National Map Viewer (https://www.usgs.gov/programs/national-geospatial-program/national-map) DEM, satellite, and land use are within the same window.

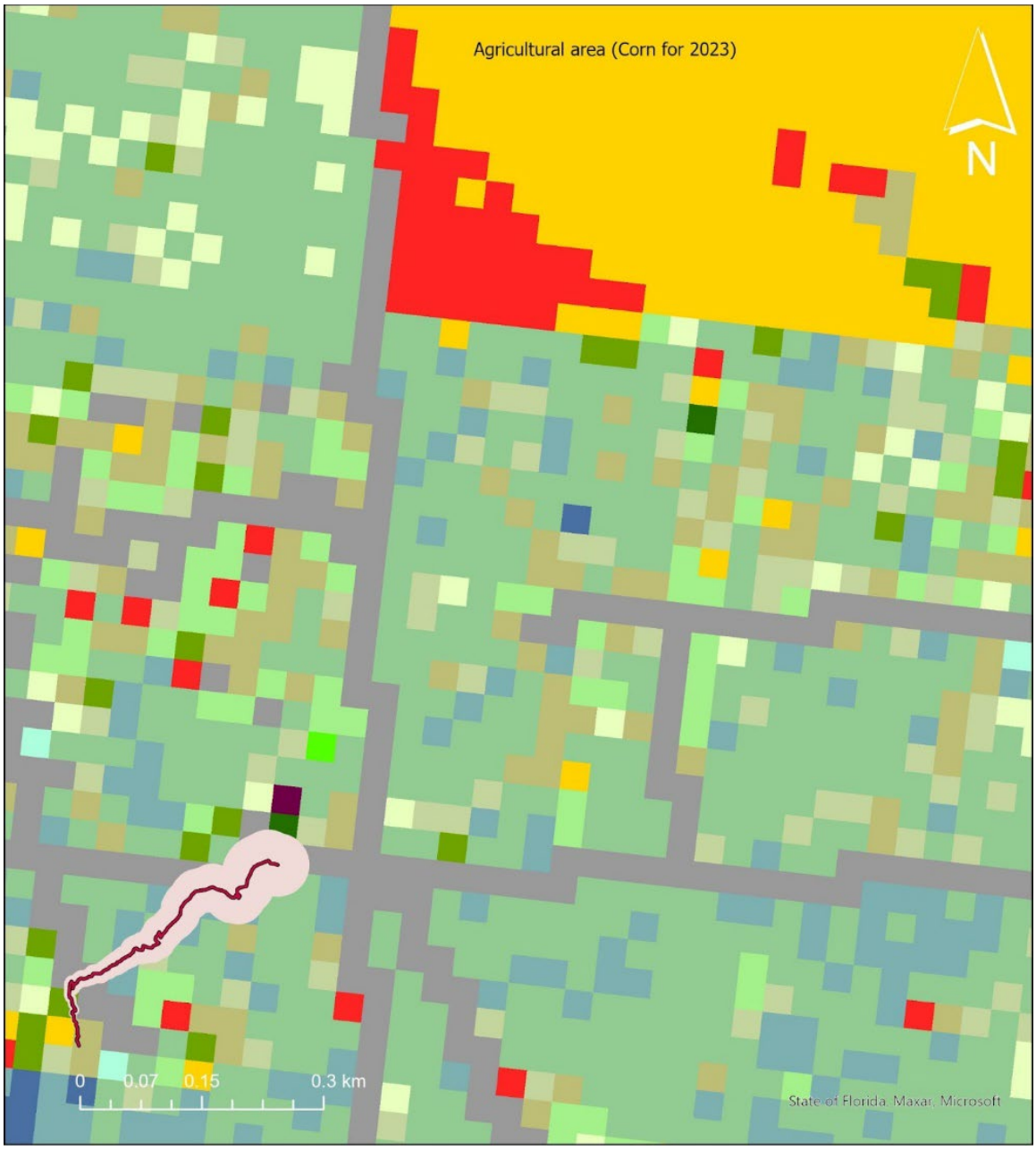

Figure 21: Land use (Cropscape 2023 (http://www.cropscape.com) and mapped conduit by SUNFISH (red line) and horizontal error (shaded pink) associated with increasing penetration. See Figure 9 for land use categories within this domain.

Nitrate

The nitrate values for each sample collected in the cave were extracted from the continuous nitrate sensor data and compared to the NO_3-N results from Advanced Environmental Laboratories (AEL) (Table 9). The full continuous nitrate .csv from the SUNA is supplied as a deliverable, but the site-specific values (Figure 19) were extracted and are reported below for each site. Additionally, SUNFISH validated the SUNA sensor before and after deployment, and the results of that validation is provided in APPENDIX D.

Analyte	Unit	MDL	Vent	Site 1	Site 2 (Farthest)
NO_3-N (SUNA)	mg/L	0.01	4.10	4.14	4.15
NO_3-N (AEL)	mg/L	0.45	3.70	3.80	3.90
DOC (AEL)	mg/L	0.50	0.51	0.50	0.50
Turbidity (AEL)	NTU	0.13	0.46	1.20	0.55
Color (AEL)	CU	5	5	5	5

Table 9: The values for the nitrate values and water quality parameters.

The SUNA sensor has an accuracy of 10% of the sample reading (error) at nitrate concentrations < 10 mg/L-N (SUNA manual Revision J), and the error reported by the lab based on laboratory standard and duplicate was 1.7% (APPENDIX E). The nitrate reported by the SUNA sensor and laboratory values matched within the accuracy ranges expected for the SUNA (Figure 22). The trends were also captured, as nitrate appeared to slightly increase from the vent to the final sample location.

Parameter	Site 1	Site 2	Vent
DO (mg/L)	6.93	6.98	7.02
Temperature (°C)	20.86	20.86	20.85
pH	7.58	7.58	7.57
Conductivity/Specific Conductance (µS/cm)	263/285	261/283	263/286
Depth (m)	27	25	6

Table 10: Values of water quality measurements recorded on the YSI EXO^2. The values are the average of 4 instantaneous values (1 minute) beginning at the start of sample collection.

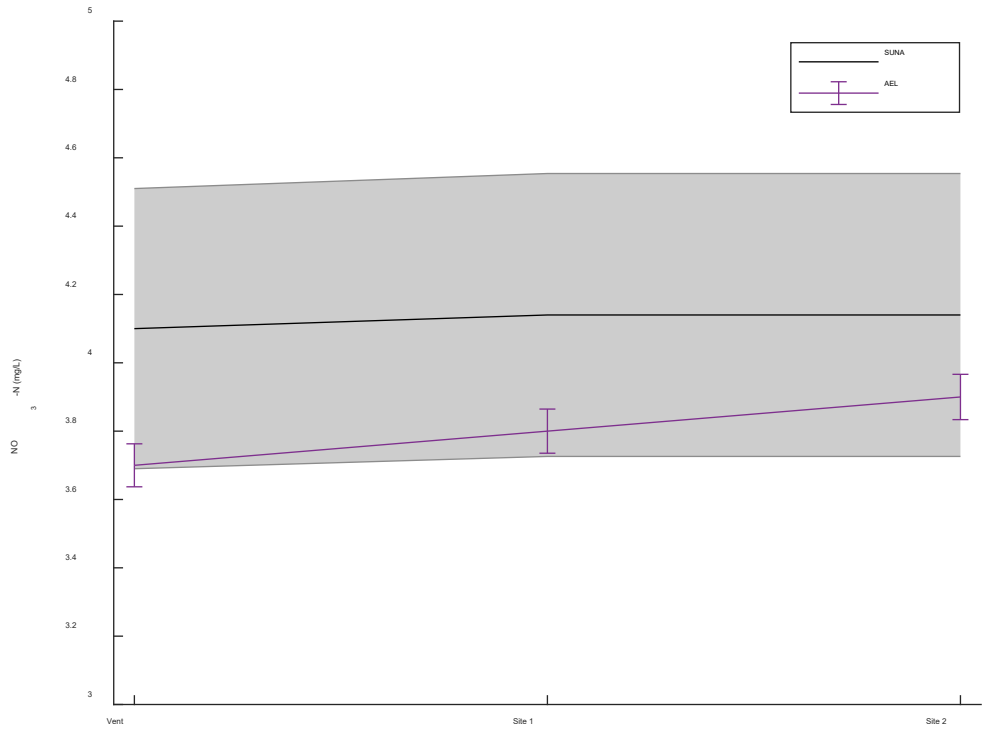

Figure 22: SUNA readings and 10% error specified by manufacturer (grey shaded region) and AEL (EPA Method 300.0) analyzed nitrate with error bars from reported RDL.

Sample collection for the first water sample began at approximately 7:43 am and the second sample at approximately 9:46 am (See Figure 19 for locations). Vent sample collection began (purge) as SUNFISH exited the cave at about 11:15 am. Water sample collection began at ~11:30 and ended ~11:40 am. The approximate time when the YSI EXO^2 intersected the sample location is shown in Figure 23. Divers exited the cave with the YSI EXO^2 later than SUNFISH as they had to go through some decompression.

The water at Jackson Blue Spring is clear, and both color and DOC were at detection limits while turbidity was detectable, but low and unlikely to cause interference (see Pellerin et al., 2013). It is possible the higher turbidity at Site 2 was due to kick up of silt from the divers, but at the measured values, the effects are known to be negligible. Therefore, there was no interference that needed to be accounted for when interpreting the nitrate values reported by the SUNA sensor.

Conductivity

The NBOSI C/T reports conductivity without temperature correction. We report the results of both conductivity and specific conductance because specific conductance standardizes the conductivity at a temperature of 25°C and normalizes it for temperatures being read from each sensor.

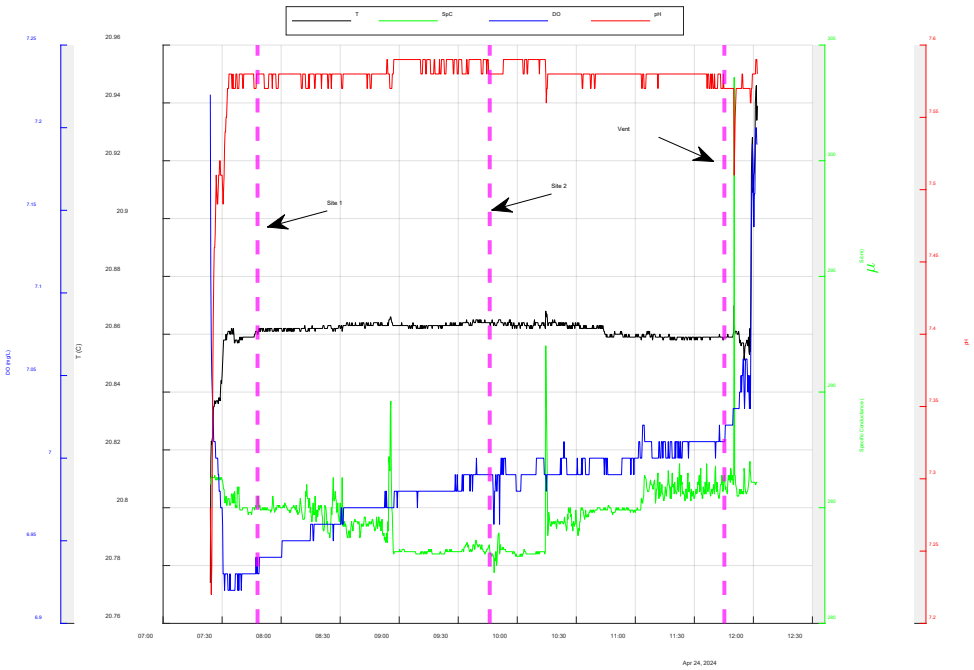

Figure 23: YSI sample data for long deployment when water samples were collected to verify nitrate readings and quantify interference. Labels indicate the time when the sample was collected and the sample location. Vent is an approximation based on diver

To convert conductivity to specific conductance (Equation 2), a linear assumption is made regarding conductivity changes from temperature (Wagner et al., 2006). The correction factor (r) applied is referenced to a KCl (Postassium Chloride) standard and is equal to r = 0.02 (vanEssen CTD Manual)

$$Specific\ Conductance = \frac{Conductivity}{1 + r(T - 25)}$$ Equation 2

The conductivity and specific conductance reported by SUNFISH fell within the ranges reported by the YSI EXO^2 but not the vanEssen CTD (Figures 24 and 25). The reported accuracy for the YSI EXO^2 conductivity is 0.5% of the reading up to 100 mS/cm (100,000 µS/cm), while for temperature the accuracy is 0.1° C. For the vanEssen, accuracy for conductivity is 1% of the value

and temperature is also accurate to within 0.1° C. Temperature for the NBOSI C/T matched almost identically with the YSI EXO^2 (Figure 26). The vanEssen temperature was a little higher but may have had to do with being mounted directly to the robot and potentially capturing some interference from SUNFISH operations. The RMSE's are provided in Table 11. The vanEssen comparison of readings to the standard was low, which likely explains the low values reported in the cave.

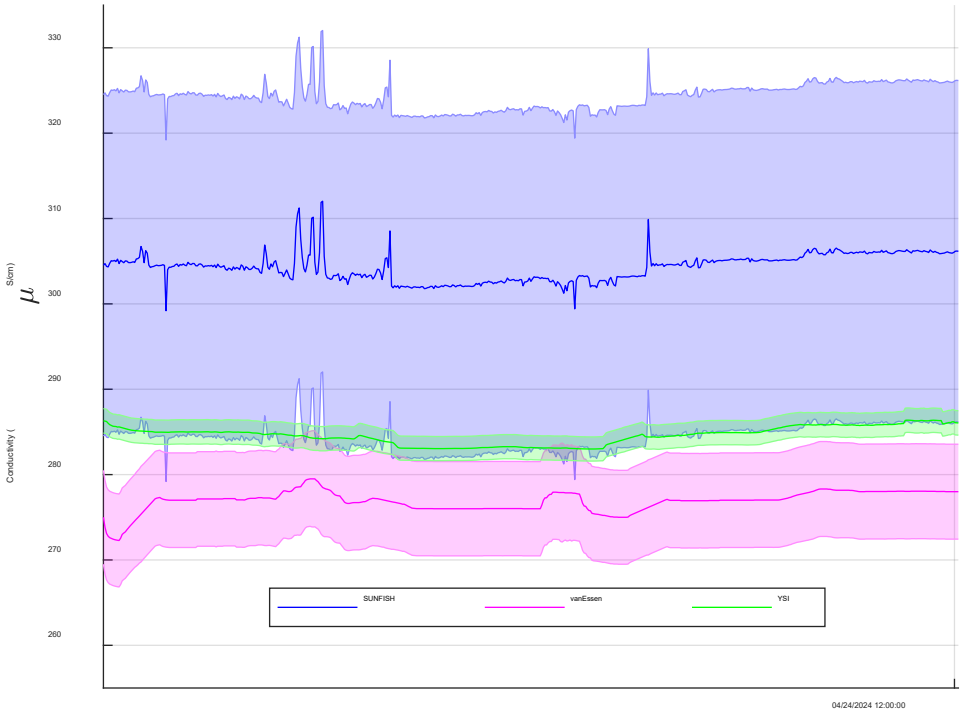

Figure 24: Conductivity comparisons between SUNFISH CTD, vanEssen, and YSI EXO^2. Shaded error bars represent the reported accuracy of each sensor. For NBOSI C/T (on SUNFISH), the reported accuracy was 0.2 mS/cm (or 20 µS/cm) (Table 4).

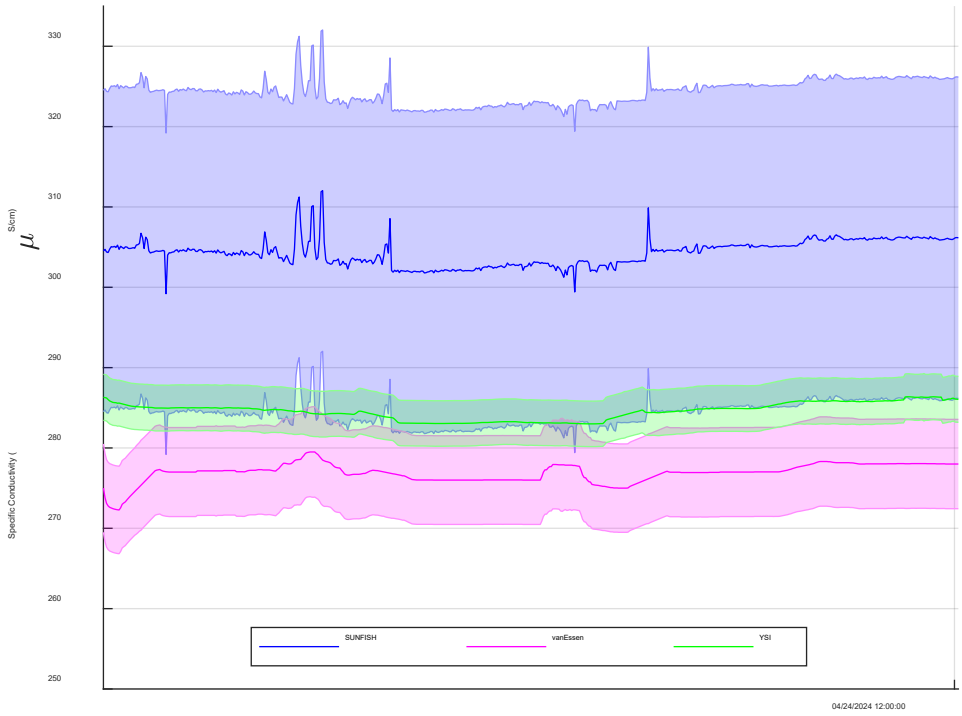

Figure 25: Specific conductance comparisons between SUNFISH CTD, vanEssen, and YSI EXO^2. Shaded error bars represent the reported accuracy of each sensor. For NBOSI C/T (on SUNFISH), the reported accuracy was 0.2 mS/cm (or 20 µS/cm) (Table 4).

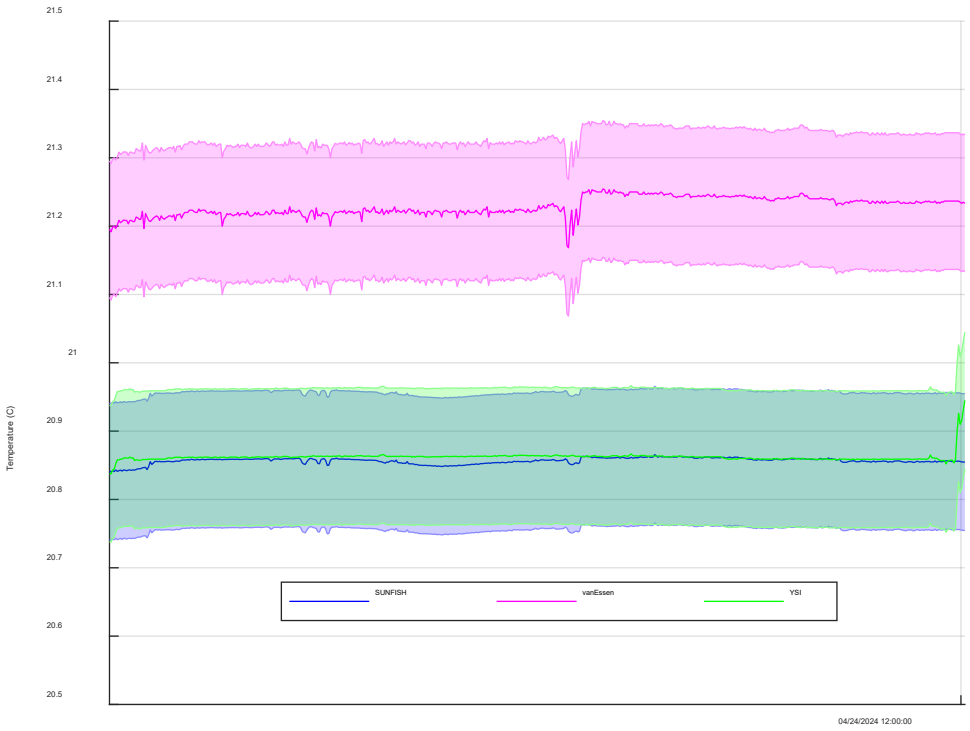

Figure 26: Temperature comparisons between SUNFISH CTD, vanEssen, and YSI EXO².

Parameter	RMSE vanEssen*	RMSE YSI
Temperature (C)	0.372*	0.009
Specific Conductance (µS/cm)	27.45	19.71
Conductivity (µS/cm)	23.12	17.01

*Table 11: RMSE's over the entire dive for each parameter. *There could have been an influence with measuring temperature on the AUV.*

In general, nitrate, conductivity, and temperature did not change much at Jackson Blue Spring, which was expected. However, there was a potential increase in nitrate from the vent to the penetration limit. The lower value at the vent could be from dilution due to fractures that have been observed delivering water to the conduit (James Draker-cave diver; personal communication), or it could be from some nitrate reduction via the sediments. However, substantial oxygenation of Jackson Blue Spring suggests it is likely additional water mixing along the conduit flowpath.

WATER SAMPLING AT MERRITT'S MILL POND

The DEP also funded additional work to collect water samples at springs that discharge to Merritt's Mill Pond. The collected water samples were similar to samples collected in 2011, which aimed to identify primary sources of nitrate to several springs discharging to Merritt's Mill Pond (see Barrios, 2011).

Site description

Merritt's Mill Pond is a 202-acre springfed dammed lake that is located in Jackson County, FL. Multiple springs provide discharge to Merritt's Mill Pond, and Jackson Blue Spring is the largest contributor (~70%), while smaller springs such as Twin Caves, Indian Washtub, Hole in the Wall, Gator Hole, Shangri-La, Hidey Hole, and Lamar's Landing provide most of the remaining 30% (Barrios, 2011, Dodson, 2013). Jackson Blue Spring serves as the primary headwaters to the lake and the other springs support the lake discharging either on the north or south side.

Nitrate concentrations have been increasing at springs discharging to Merritt's Mill Pond for the last several decades (Figure 27). At Jackson Blue Spring, average nitrate concentrations are 3.4 mg/L-N (1980-2000) with the most recent laboratory value at 3.7 mg/L-N (Table 9), while historically, nitrate concentrations were ≤ 0.5 mg/L in the 1960's. Nitrate concentrations at other springs are not as well represented in the sampling record (Figure 28) but average concentrations for 2006-2011 range from near 1 to over 3 mg/L. The primary cause of nitrate concentration increases is likely from agriculture (Katz, 2004), as the region is mostly rural and upgradient land use within the identified priority region is largely used for agriculture (Figure 9). Nitrogen isotope data of nitrate collected in 2004 and 2011 from springs around Merritt's Mill Pond indicated nitrate was from a mixture of inorganic and organic fertilizers contributing to nutrient loads (Katz, 2004, Barrios et al, 2011). Furthermore, Jackson Blue Spring's specific conductance, potassium, sulfate, and nitrate show time dependent covariance, which further suggests agricultural impairment (Figures 29, 30). The cave for Jackson Blue likely runs underneath the farm, which is ~1.3 km (as the crow flies) from Jackson Blue vent (Figure 21).

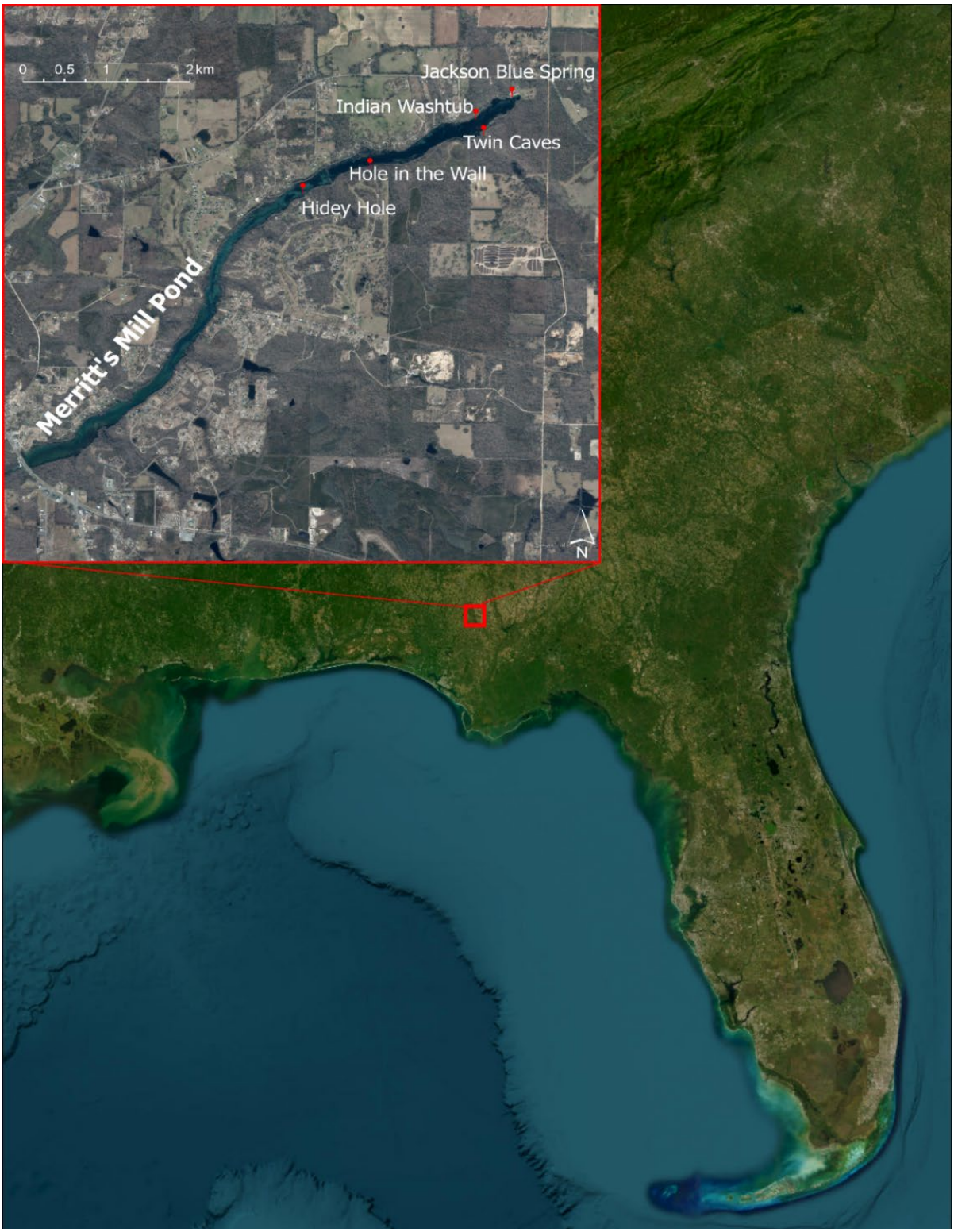

Figure 27: Location of Merritt's Mill Pond and the 5 sampled springs for this project. Hole in the Wall, Hidey Hole, and Twin Caves discharge from the south, while Jackson Blue and Indian Washtub discharge from the north end of the basin.

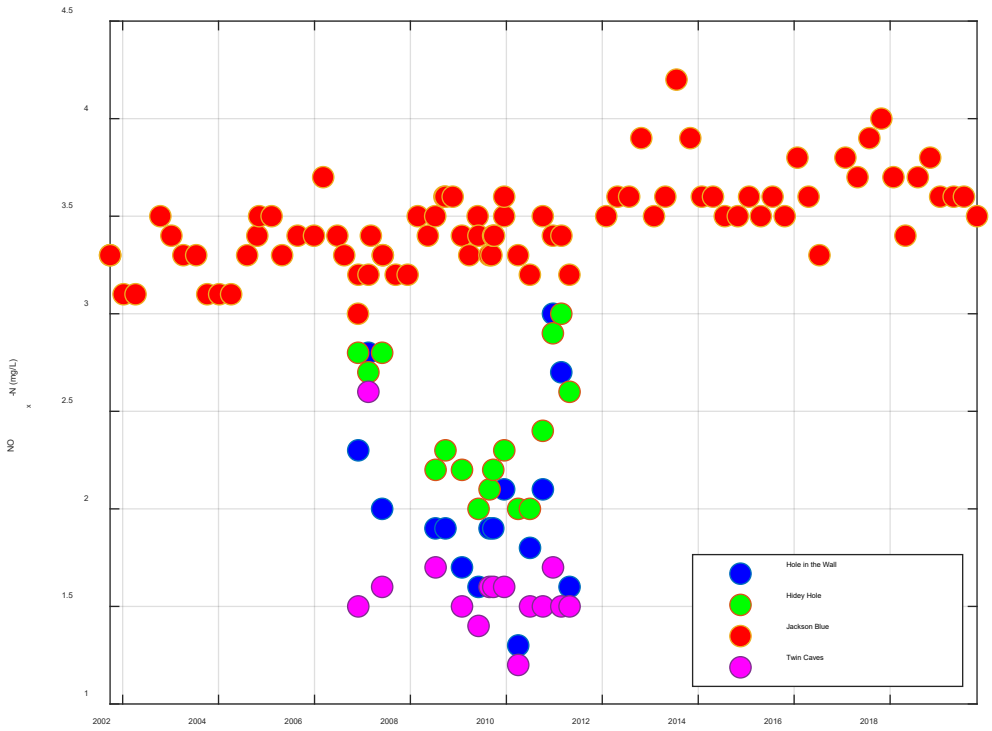

Figure 28: Nitrate (as nitrate+nitrite as nitrogen) concentrations at 4 springs discharging to Merritts' mill Pond. Data obtained from Northwest Florida Water Management District via email (Correspondence: James Sutton).

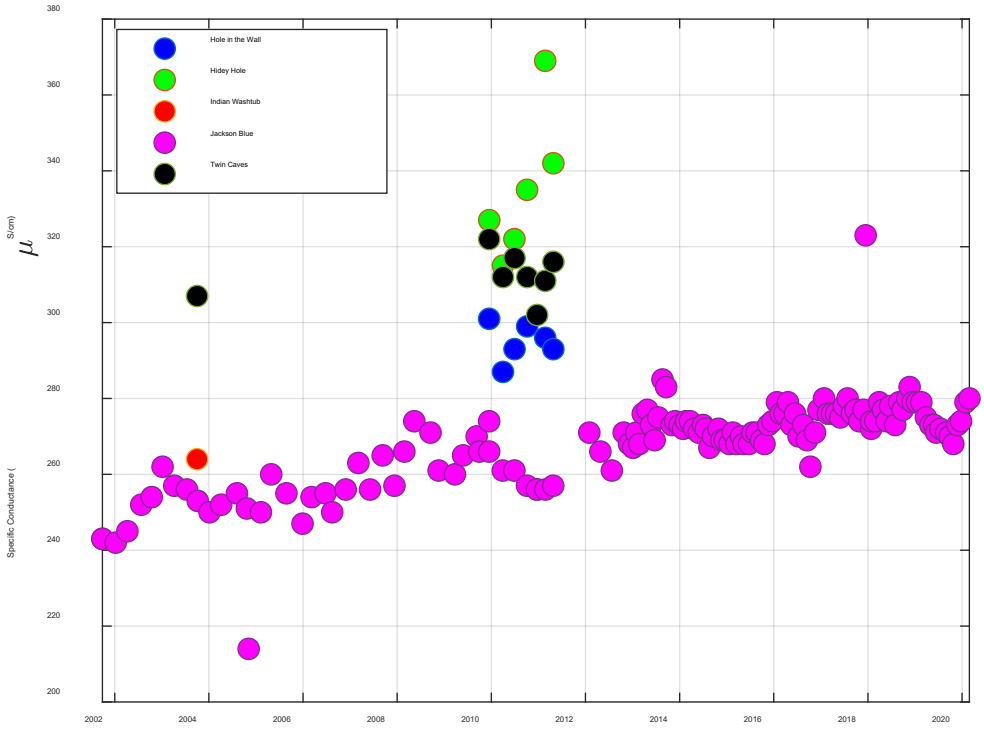

Figure 29: Specific conductance for the 5 selected springs studied for this report. Data obtained from Northwest Florida Water Management District via email (Correspondence: James Sutton).

Figure 30: Jackson Blue nitrate, specific conductivity (SpC), potassium (K), and sulfate (SO4) values for the historical record. Data obtained from Northwest Florida Water Management District via email (Correspondence: James Sutton).

Dye tracing conducted in 2015 found variable land uses contributed to different springs discharging to Merritt's Mill Pond (Table 12). Rhodamine WT, Eosine, and Fluorescein dye were injected at 3 different sinkholes which were located on land parcels nearby. Rhodamine WT was injected into a sinkhole within a wooded cattle pasture, Fluorescein dye was injected into a sediment plugged sinkhole on an agricultural property, while Eosine dye was injected into a Pelts swallet which receives storm runoff from a residential area. The results showed that Rhodamine WT (cattle) was detected at Jackson Blue Spring and Indian Washtub Spring. However, maximum detected concentrations at Indian Washtub Spring (< 0.015 ppb) were small compared to Jackson Blue Spring (441 ppb). The Eosine dye was detected at Hole in the Wall and Twin Caves at maximum concentrations of approximately 3.66 and 4.73 ppb, respectively. Fluoroscein dye was not detected at any spring, however irregular fluorescence peaks occurred at Jackson Blue Spring which could indicate that Fluoroscein was emerging due to overlapping wavelengths, but not in quantifiable enough amounts. It was noted that the emergence of Eosine dye occurred on springs that discharge on the south side of the pond, whereas Rhodamine WT dye emerged at springs discharging on the north side of the pond. Thus, it was clear that Jackson Blue Spring and Indian

Washtub Spring could receive water from different groundwater contributing areas than Hole in the Wall and Twin Caves. The potentiometric surface map for the UFA indicates aggregation of water from different land areas.

Site	Land use association (dye trace)	Sampling protocol	Analytes for FDEP	Analytes (USF)*	Justification
Jackson Blue	Cattle and possible Agriculture	Surface water sampling	$\delta^{15}N$ and $\delta^{18}O$ of nitrate and nitrate	Major ions, trace metals (Fe, Mn), Water isotopes	Found Rhodamine and potentially Fluorescein. Behaves similar to Shangri-La. So Shangri-La may be redundant
Indian Washtub	Cattle				Found Rhodamine, but definitely not Fluorescein. Is a potential end member for just the cattle.
Hidey Hole	Unknown				Not dye traced, but previous $\delta^{15}N$ shows values similar to Twin Caves, with same nitrate as Gator Hole. Also, based on age dating, the youngest water of all sites sampled according some dating methods.
Twin Caves	Storm runoff				Eosine dye emerged. No other dyes
Hole in the Wall	Storm runoff				Water quality is apparently the most dynamic according to Edd Sorenson. Eocene dye emerged.

Table 12: Justification for each site selected and previous results of dye tracing and studies. Additionally, the analyses to be done are also reported.

Based on previous dye tracing and historical geochemistry collected at springs around Merritt's Mill Pond, we selected 5 springs (see Figure 27) for analysis. We collected major ions (anions and cations), metals, nitrogen and oxygen isotopes of nitrate, NO_x-N, and hydrogen and oxygen isotopes of water. In summary, we selected springs that were likely draining different land uses and on different sides of the pond and spanned a range of nitrate concentrations. Additionally, groundwater ages estimated at each spring were also considered in the selection, with springs representing the youngest water (Hidey Hole), the oldest water (Jackson Blue), and a few with ages that fell between. We also sampled Indian Washtub Spring, which had not been sampled previously for isotopes, but had been dye traced and is located on the north side of Merritt's Mill Pond, directly across from Twin Caves.

Methods

We used a pontoon boat rented from Cave Adventurers to navigate to the springs on Merritt's Mill Pond. We used GPS and confirmation from divers to locate each one of the springs. We sampled for metals (Fe (Total), Mn^{2+}, Sr^{2+}), major cations (K^{+}, Na^{+}, Mg^{2+}, Ca^{2+}), major anions (Cl^{-}, SO_4^{2-}), alkalinity (as $CaCO_3$), NO_x-N, nitrogen ($\delta^{15}N$) and oxygen ($\delta^{18}O$) isotopes of nitrate, and hydrogen ($\delta^{2}H$) and oxygen ($\delta^{18}O$) isotopes of water.

For water sampling, we used a Geotech peristaltic pump with PVC tubing to collect all water samples. The tubing was lowered as close to the vent as possible, with personnel entering the water to ensure the tubing was in the vent. The end of the tubing was taped to a calibrated YSI ProDSS, which reports dissolved oxygen, pH, temperature, turbidity, specific conductivity, and depth and these values were recorded after stabilization. A 0.45-micron filter was used for metals, major cations, NO_x-N, and nitrogen ($\delta^{15}N$) and oxygen ($\delta^{18}O$) isotopes of nitrate, a 0.22 micron filter was used for hydrogen ($\delta^{2}H$) and oxygen ($\delta^{18}O$) isotopes of water and alkalinity was unfiltered. Metals and major ions were collected in HDPE bottles and preserved with 0.5M HNO_3 to a pH of 2. NO_x-N and nitrogen ($\delta^{15}N$) and oxygen ($\delta^{18}O$) isotopes of nitrate were sampled into 125mL HDPE bottles. NO_x-N was preserved with 12M HCl to a pH<2 while samples for nitrogen ($\delta^{15}N$) and oxygen ($\delta^{18}O$) isotopes were not acid preserved, but frozen within 24 hours. Anions, alkalinity, and water isotopes were unpreserved. All samples were analyzed within DEP mandated hold times.

Metals, major ions, water isotopes, and alkalinity were analyzed at USF's geochemical facilities. Metals and cations were analyzed on a Perkin Elmer Avio 200 inductively coupled plasma optical emission spectrophotometer (ICP-OES) using EPA method 200.7 for analysis. Alkalinity was titrated using a Hanna Instruments automatic alkalinity titrator. The titration method uses 0.02N sulfuric acid to titrate to an end point of pH 4.5. Anions are determined using Ion Chromatography (IC) and EPA method 300.0. Water isotopes are analyzed on a Picarro L2130-I cavity spectrometer and are within 0.2 ‰ precision.

Nitrogen ($\delta^{15}N$) and oxygen ($\delta^{18}O$) isotopes of nitrate and NO_x-N were shipped overnight to the Nebraska Water Center at the University of Nebraska-Lincoln (UNL). NO_x-N was analyzed using a Seal Analytical AQ2 Discrete Analyzer using EPA Method 353.2 Rev 2.0 (1993). Nitrogen ($\delta^{15}N$) and oxygen ($\delta^{18}O$) isotopes of nitrate were analyzed using the titanium reduction and conversion to N_2O for isotope analysis (Altabet et al., 2019) and stable isotopes are analyzed on a GV Instruments Isoprime Dual Inlet Isotope Ratio Mass Spectrometer interfaced with a Tracegas Pre-Concentrator flow analyzer.

It is noted that water isotopes, major ions, alkalinity, and trace metals are financially supported by USF and nitrate (as NO_x-N) and nitrogen ($\delta^{15}N$) and oxygen ($\delta^{18}O$) isotopes of nitrate are financially supported by DEP.

Results and discussion

Nitrogen and Oxygen isotopes of nitrate

As of this new report, the $\delta^{15}N$ and $\delta^{18}O$ isotopes of nitrate all the springs have been reanalyzed at UNL and this report has been updated to reflect the new values.

The ($\delta^{15}N$) and ($\delta^{18}O$) of nitrate were similar to $\delta^{15}N$ values obtained in previous studies, in that they indicate fertilizer is the primary origin of nitrate (Katz, 2004, Barrios, 2011). However, previous data did not obtain $\delta^{18}O$ of nitrate, and thus a more comprehensive understanding of N sources was lacking. Isotopes collected from all springs fall within the ranges for manure and septic sources as well as nitrification of N-based fertilizers (Figure 31) (Snow, 2018). The results for Jackson Blue, Twin Caves, and Hole in the Wall cluster together and are close to the outer boundaries of manure and septic sources. But of all the springs analyzed, Jackson Blue Spring falls closer to inorganic fertilizers, even if by a small amount. The proximity of Jackson Blue Spring to the farm (~1.3 km NNE of the vent), may be one of the factors driving more depleted (lower) $\delta^{15}N$ values. The overlap between "manure and septic" and "NH_4 from fertilizers" may be due to both septic and fertilizers affecting the nitrate isotope values. However, because on average, septic sources tend to be more enriched with $\delta^{15}N$ (Kendall and Aravena, 2000), it may be that fertilizers have more of an impact on nitrate concentrations than septic and this influence may be reflected in the more depleted $\delta^{15}N$ over time (Figure 32). Furthermore, a slightly elevated $\delta^{18}O$ with respect to the $\delta^{18}O$ boundaries in Figure 31, albeit minimal, may indicate a surface derived source (fertilizer, manure) whereby evaporation could enrich $\delta^{18}O$ that binds to nitrogen in the soil, whereas septic derived sources would have relatively lower $\delta^{18}O$ values (Kendall and Aravena, 2000). The land use contributions defined in Dodson, 2013, reported that 42.78% of the springshed was agriculture, 42% was forest/open rural, while only 6.34% was residential. The land use remained relatively similar for 2019 land use data, of which agriculture made up 42%, forest made up 40%, urban was 6%, and 4% was classified as utilities and transportation (https://hub.arcgis.com/datasets/FDEP::statewide-land-use-land-cover/about). Water (1%), wetlands (3%), barren land (1%) and rangeland (4%) made up the remaining land use. The correlated ion data at Jackson Blue Spring in Figure 30 may also support fertilizers being the primary cause of nitrate. However, these conclusions are not definitive, and may require further investigation.

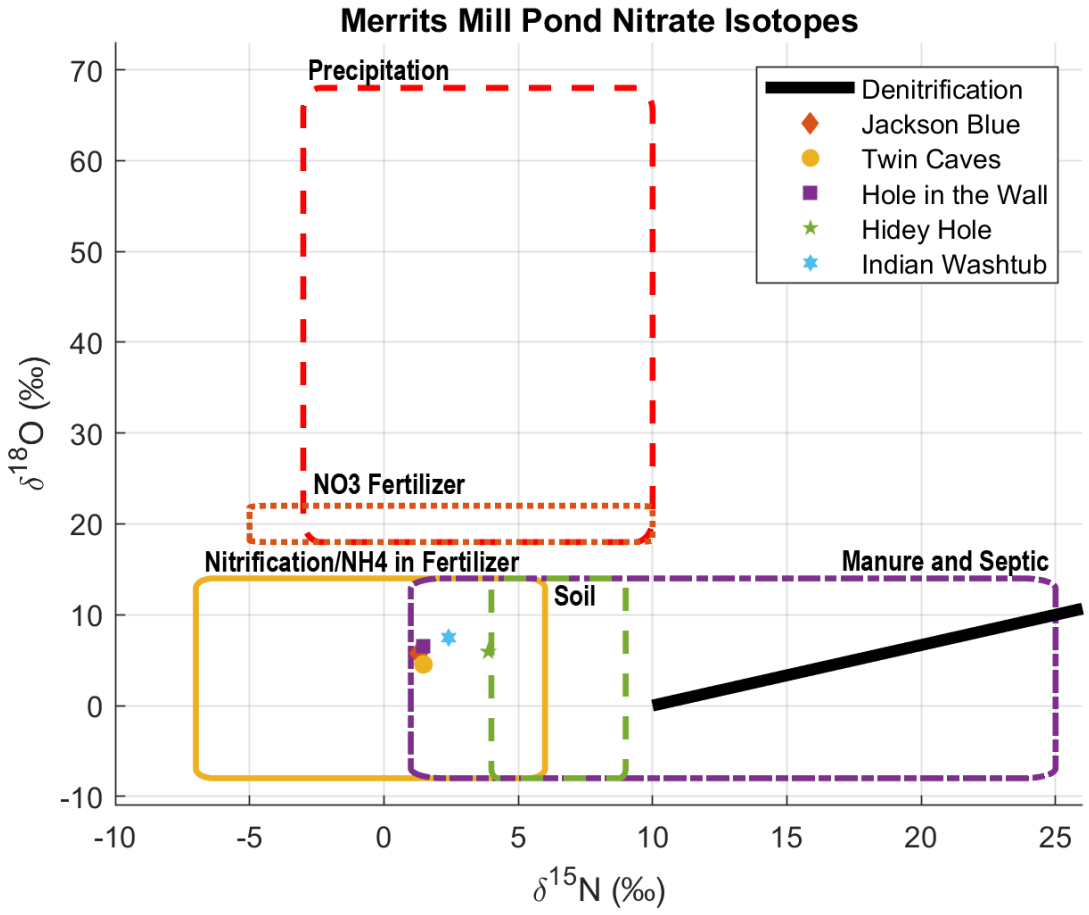

Figure 31: Boundaries established by Kendall and Aravena, 2016 and Snow, 2018. The data are a combination of references for each boundary. ***This graph has been updated from the previously submitted report.***

Data were also plotted between $\delta^{15}N$ and nitrate concentrations to quantify and visualize any relationship between nitrate concentration and source of nitrogen (Figure 32). The highest nitrate concentrations are at Jackson Blue Spring and Indian Washtub, which are both on the north (west) part of the Merritt Mill Pond region. The ranges for $\delta^{15}N$ for the 2024 sampling period are slightly lower than the samples obtained in 2011. The only exception is for Hidey Hole, which was enriched by 1.1‰ relative to 2011 sampling. The implication for the lower values in 2023 would be more influence from inorganic fertilizers, while more enriched values may have a greater influence from septic and manure. Nitrate concentrations overall had also increased for all springs analyzed and the largest increases were observed at Hidey Hole and Jackson Blue Springs.

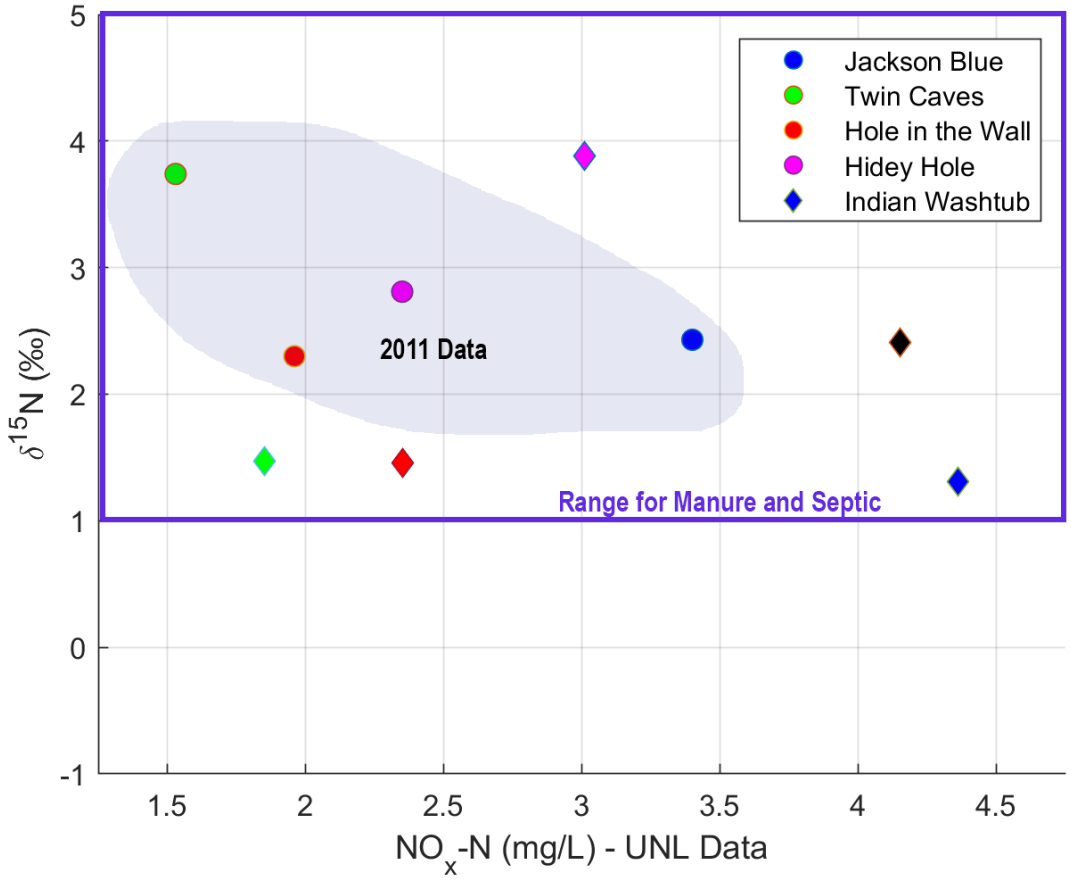

Figure 32: Nitrate (from UNL) and $\delta^{15}N$ from nitrate. The purple line is the range for manure and septic and all values fall within that range as well as the range for NH4/Nitrification which includes the entirety of the y-axis range. Colors for sites of different years are the same. For example, blue is always Jackson Blue Spring, but the diamonds indicate 2024 data. ***This graph has been updated from the previously submitted report.***

Water isotopes

The water isotopes for the current (2024) data cluster closely together (Figure 33). The isotopes are slightly more enriched with respect to δ^2H, but more depleted with respect to $\delta^{18}O$ when compared to the 2011 data. This is likely a product of seasonal differences in sampling, precision of different instruments, and a recent rainstorm that occurred which likely recharged the spring basin and caused some shifts in the average isotope values. Table 13 provides averaged water isotope data for Jackson County for reference, and during summer months, it is observed rainwater isotopes are more enriched with δ^2H and $\delta^{18}O$ than during spring and fall. It is noted that the ranges observed for $\delta^{18}O$ data points are within the Picarro instrument precision of 0.2‰.

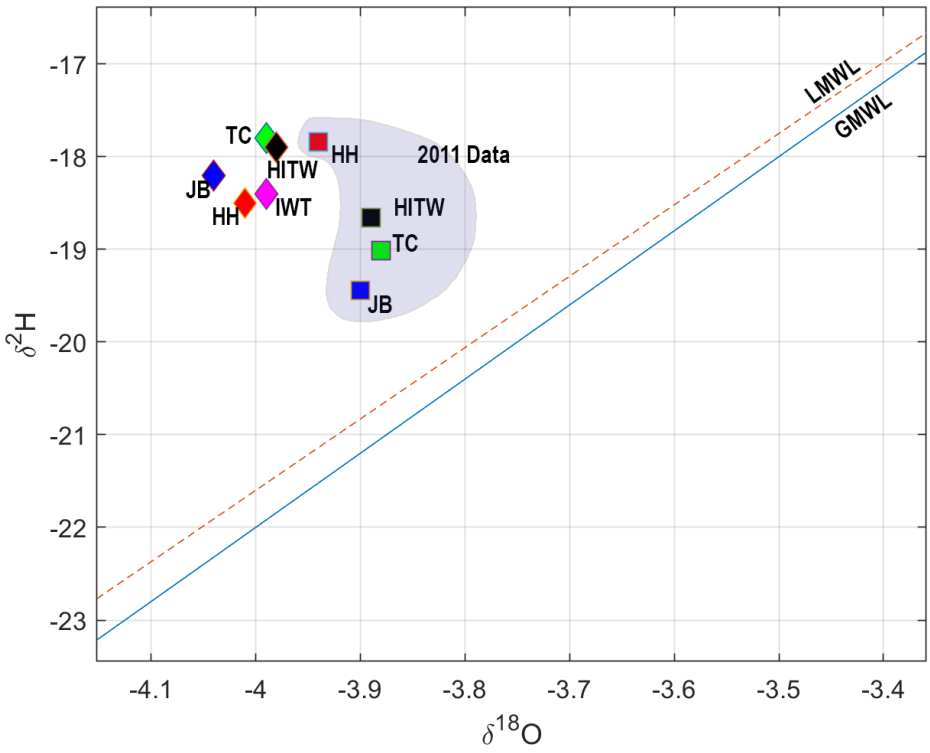

Figure 33: Water isotopes collected for this project. Diamonds are new data collected in 2024, while squares are previous data collected in 2011. HH = Hidey Hole; HITW = Hole in the Wall; JB = Jackson Blue; TC = Twin Caves; IWT = Indian Washtub. LMWL = Local Meteoric Water Line. GMWL = Global Meteoric Water Line

	Jan	Feb	Mar	Apr	May	Jun	Jul	Aug	Sept	Oct	Nov	Dec
δ^2H (‰, V-SMOW)	-30	-31	-31	-17	-5	-4	0	-1	-3	-19	-20	-28
δ^{18}O (‰, V-SMOW)	-5.1	-5.3	-5.2	-3.3	-1.7	-1.5	-0.7	-1.1	-1.5	-3.5	-3.6	-4.6

Table 13: Water isotope values for Jackson County based on month. Data was obtained from waterisotopes.org.

Additional geochemical data

Additionally, other water quality parameters were collected to aid in the interpretation of source waters and complement the isotope data (Table 11). Alongside direct interpretation, we constructed Piper diagrams to help visualize the major ion chemistry and how the different springs compared to one another. Piper diagrams to help visualize the major ion chemistry and how the water chemistry at different springs compared to one another. Piper diagrams are developed by using major ground ion concentrations (milliequivalents) and includes Ca^{2+}, Mg^{2+}, K^{+}, Na^{+}, $SO4^{2}$, Cl^{-}, and HCO_3 (Bicarbonate) values. Piper diagrams serve several purposes, including identifying

potential causes of water quality changes such as from seawater intrusion, anthropogenic influence over time, and to compare natural similarities (i.e. geologic) between source waters. Data are plotted on the two bottom ternary diagrams and projected onto the upper triangle for the classification of source waters (Figure 34a). When plotting these data over time, the causes of changes in water quality can sometimes be identified by how the data points migrate across the triangular diagram over time (Figure 34b). For the purposes of this report, the Piper diagrams are used with the newly collected data to compare water similarity. Unfortunately, there was not enough data from the historical record for all the sampled sites to plot more than one data point for each, so only the most recent data collected was used.

Figure 34a: Water type interpretation for Piper diagrams. Carbonate systems fall within the "Magnesium-Bicarbonate" type water class. Example arrows drawn for projection.

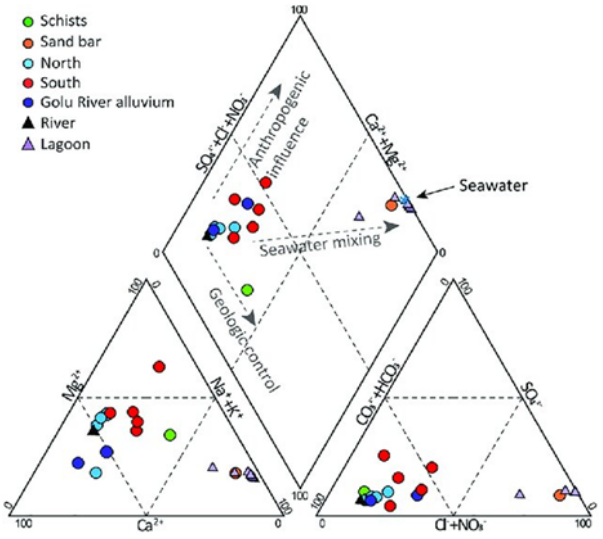

Figure 34b: Interpretation of data plotted on Piper diagrams when multiple samples of the same data are plotted (or several series compared). The dotted lines indicate the trajectory the data will plot when anthropogenic (contaminant) or seawater intrusion occur. When geologic changes occur, that can be demonstrated as well.

There was a clear difference in water chemistry between springs that discharge to the north and south of Merritt's Mill Pond. The data support the drainage of different land uses and potentially some variability in geology. Nitrate values at Indian Washtub and Jackson Blue Springs show much higher nitrate concentrations, which is potentially from the farm upgradient of Jackson

Blue. Additionally, Hole in the Wall is an extensive cave system that is mapped underneath Merritt's Mill Pond and extends over to the north side of the pond (Figure 35). A very shallow section of Hole in the Wall cave is located on the extreme northeast side of Merritt Mill Pond and contains speleothems, which are rare if almost never found in Florida's phreatic caves. This indicates dry condition recharge, which could be due to lowering the levels in the pond or could be a constraint on paleo-water tables. This cave extent and morphology leads into the chemistry interpretation, as the water chemistry at Hole in the Wall has more in common with springs on the southern side of Merrit Mill Pond based on most geochemical parameters (Table 14). However, some ion concentrations do appear to fall between the two end members including the nitrogen isotope value (Figure 31), overall water chemistry in Piper Diagrams (Figure 36) and specific conductance (Table 14). Therefore, Hole in the Wall, could potentially discharge water that is sourced from both the north and south sides of Merritt's Mill Pond.

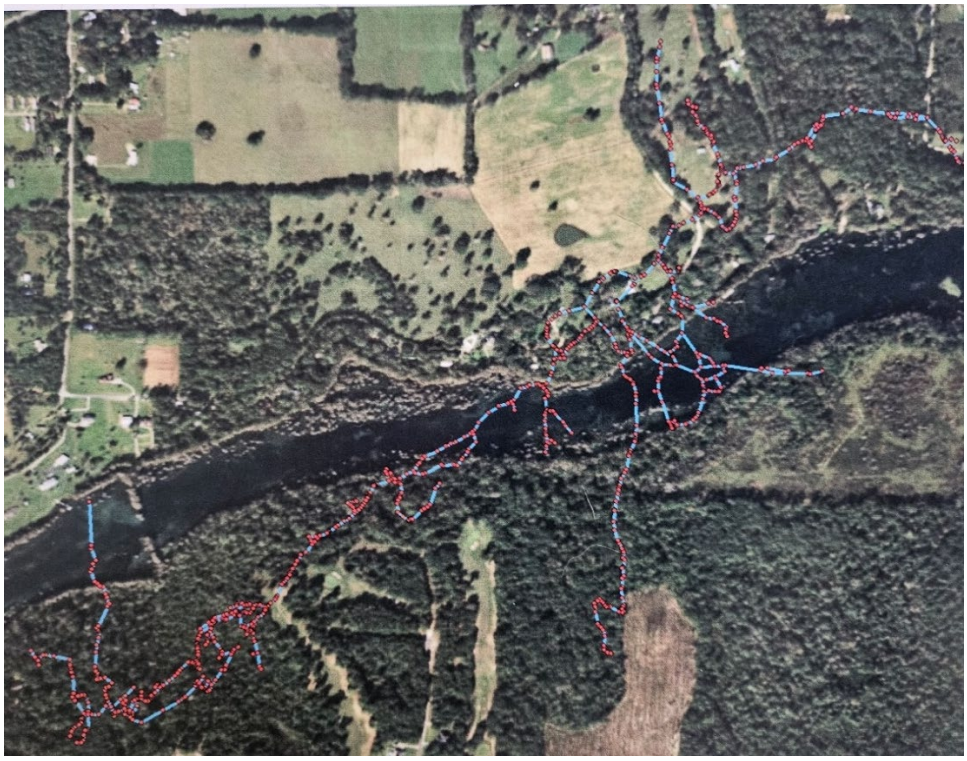

Figure 35: Hole in the Wall cave map. Note that the cave runs underneath Merritt's Mill Pond, though the vent sampled was sampled where it discharges to Merritts' Mill Pond on the south side. Image courtesy Cave Adventurers. Flow directions are on original map (personal copy).

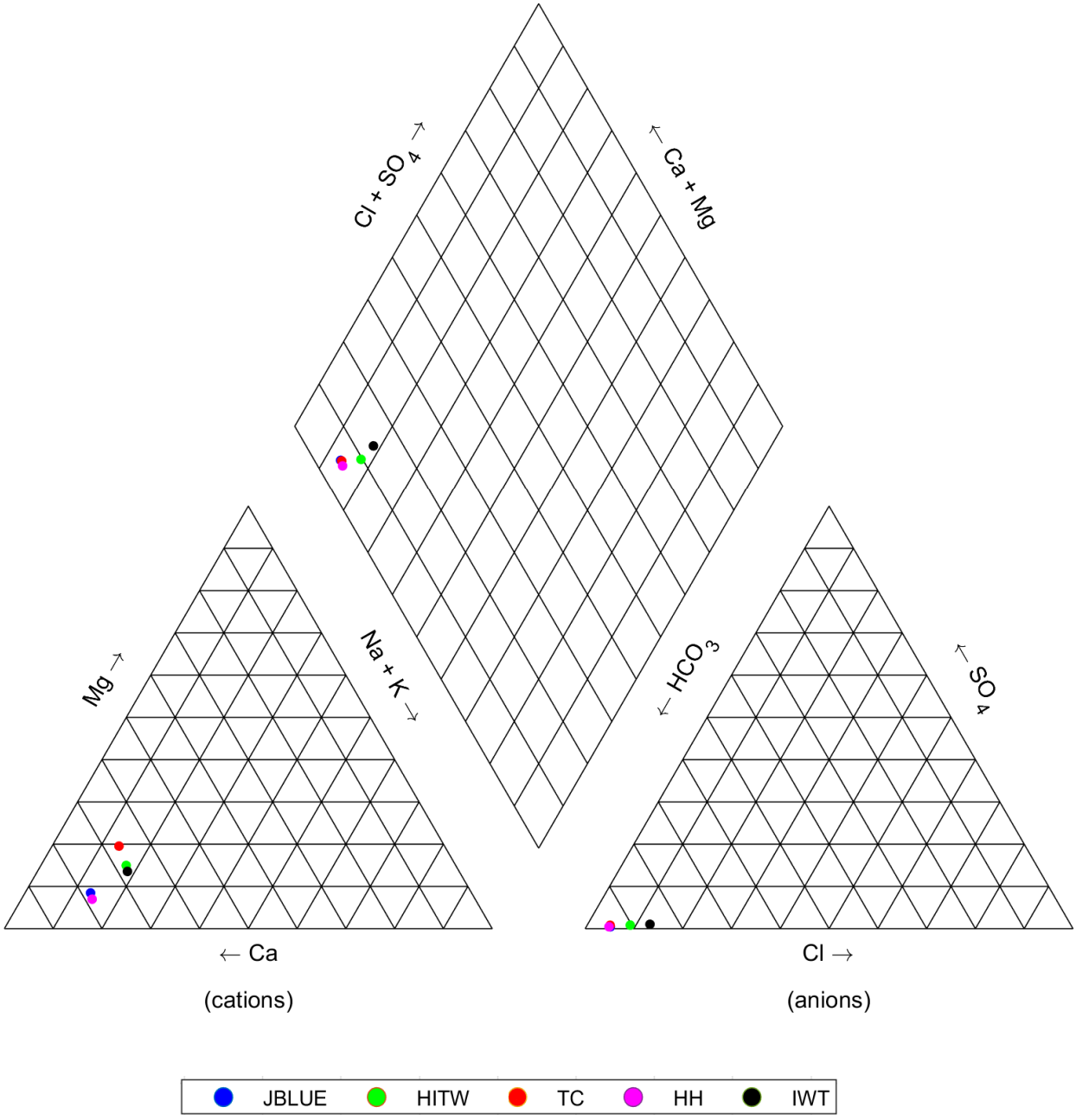

Figure 36: Piper diagram constructed from major ion chemistry (Table 14).

Analyte	Unit	Jackson Blue	Hole in the Wall*	Twin Caves*	Indian Washtub	Hidey Hole*
Major ions and metals						
Ca^{2+}	mg/L	45.95	46.67	51.86	47.52	50.72
Mg^{2+}		3.02	6.27	9.21	2.56	6.13
Alkalinity ($CaCO_3$)		142.8	158.8	194.7	114.1	143.0
HCO_3 (Calculated)		174.3	193.7	237.5	139.2	174.4
Na^{+}		1.55	2.75	2.37	1.78	3.20
Cl^{-}		5.45	10.20	5.22	5.13	15.47
K^{+}		1.22	1.22	1.17	1.25	1.27
SO_4^{2-}		2.64	5.29	4.82	2.74	6.83
Fe^{2+} + Fe^{3+}	µg/L	5	4	6	284	233
Mn^{2+}		18	19	19	21	20
Sr^{2+}		19	35	49	19	57
YSI data						
DO (mg/L)	mg/L	6.85	5.23	5.66	6.87	6.43
Specific conductance	µS/cm	285	312	348	296	340
Temperature	C	20.9	20.5	20.5	21.2	20.9
pH	--	6.88	7.4	7.28	6.87	6.8
All Nitrogen data						
NO_x-N (UNL)	mg/L	4.36	2.35	1.84	4.15	3.01
NO_x^--N (USF) SP		3.7	2.04	1.65	3.47	1.98
NO_3^--N (USF) IC		3.3	1.91	1.28	3.46	2.31
NO_3^--N (AEL)		3.7	--	--	--	--
NO_3^--N (SUNA)		4.10	--	--	--	--

Table 14: Geochemical parameters for the sampled springs. Blue shaded text are springs discharging from the south side of Merritt's Mill Pond. Nitrate concentrations from data collected at AEL are also shown for Jackson Blue.

SUMMARY AND FUTURE WORK

The project team integrated the new payloads onto the SUNFISH AUV and collected valuable data on water quality, conduit geometry, conduit location, and depths at Jackson Blue Spring. USF collected water quality data that validated SUNFISH nitrate, salinity, and temperature water quality sensors, and collected geochemical data to evaluate water quality changes and sources of pollution to Merritt's Mill Pond. The deliverables and results of the project have been provided to the FDEP via digital transfer and/or in this report.

Delicate aquatic ecosystems in springs, lakes, and rivers that are balanced by the water chemistry and quantity emerging from the Floridan Aquifer have been disrupted by human alterations to groundwater quality and storage. These disruptions not only impact ecosystem health, but also economic viability from activities including general tourism, fishing, diving, and swimming. Preserving and restoring water quality and quantity is therefore a high priority for the state of Florida, and continued work to improve our knowledge of complex karst aquifers is necessary for implementing effective water resource strategies.

SUNFISH can help Florida achieve water quality restoration and preservation goals by mapping and monitoring water quality in places challenging to access, create spatial maps of conduit geometry, hydraulics, and water quality parameters, improve flow and transport modelling, and advance groundwater science through data collection. Future work for SUNFISH would be to complete a more comprehensive water quality and 3-D mapping of cave systems that support springs of high economic and ecological value such as Wakulla Springs and surrounding sinks, Manatee Spring, Lafayette Blue Spring; among other priority cave systems. Additionally, new discrete water sampling technology has been integrated on SUNFISH and could be adapted to collect discrete water samples in caves and further advance its capabilities. SUNFISH can also be used to map other caves and sinkholes to explore potential leads, connect cave passages, and identify source water pollutants.

A late project funding start and problematic hydraulic conditions in the compressed deployment window were not ideal for SUNFISH testing and the required diver support. Unfortunately, the compressed deployment window pushed operations into when many Florida springs become undivable due to seasonal spring storms that cause reversals or increased spring discharge due to recharge. However, part of the compressed deployment window was due to the integration of the nitrate sensor, which reduced the timeframe SUNFISH could be deployed within the fiscal year. Future work would include control points such as groundwater wells, sinkholes, or karst windows which can be used to validate navigation and convert pressure into hydraulic head

data providing more interpretable hydraulic gradient maps. Fortunately, many priority springs have karst window and sinkhole access points, and some have surveyed wells or pump houses within the conduit that can be used as control points. Further, external validation techniques can be used including radiolocation which has been employed at several caves, including Wakulla Springs. Current post-validation of the Jackson Blue Spring cave map is underway using radiolocation provided by the Woodville Karst Plain Project cave divers. Further, the SUNFISH AUV can be upgraded with additional features (such as a more hydrodynamic faring, updated navigation sensors, and improved control laws) to enable mapping in higher flow, shrinking the minimum cave diameter for mapping operations (currently 2 m), or even eliminating the need for a tether for human supervision. These features can greatly enhance what can be done with SUNFISH, and the possibilities for future karst research.

REFERENCES

- ASPRS Positional Accuracy Standards for Digital Geospatial Data, Edition 2 (2023)
- Ballard, R.D., Mayer, L., Broad, K., Richmond, K. and Shapiro, B., 2020. Sea caves of the Channel Islands. *Oceanography (Washington, DC)*, *33*(1), pp.34-35.
- Barrios, K., 2011 Nitrate Source of Springs Discharging to Merritt's Mill Pond, Jackson County, Florida. Technical Report prepared for the Northwest Florida Water Management District.
- Brown, A.L., Young, C. and Martin, J.B., 2016. Groundwater-surface water interactions in the Suwannee River basin. *Florida Scientist*, pp.220-238.
- Budd, D.A. and Vacher, H.L., 2004. Matrix permeability of the confined Floridan Aquifer, Florida, USA. *Hydrogeology Journal*, *12*, pp.531-549.
- Dodson, J. 2013. Nutrient TMDL for Jackson Blue Spring and Merritt's Mill Pond. Technical Report prepared for the Florida Department of Environmental Protection.
- Dreybrodt, W., Gabrovsek, F. and Siemers, J., 1999. Dynamics of the early evolution of karst. *Karst Modelling (eds AN Palmer, MV Palmer and ID Sasowsky), Special Publication*, *5*, pp.106-19.
- Florea, L.J., 2006. The karst of west-central Florida.
- Hegrenaes, O.; Saebo, T.O.; Hagen, P.E.; Jalving, B. Horizontal Mapping Accuracy in Hydrographic AUV Surveys. In Proceedings of the IEEE AUV Conference, Monterey, CA, USA, 20–23 September 2010
- Jalving, B. "Depth Accuracy in Seabed Mapping with Underwater Vehicles," in Oceans, 1999.
- Kincaid, T.R. and Werner, C.L., 2008. Conduit flow paths and conduit/matrix interactions defined by quantitative groundwater tracing in the floridan aquifer. In *Sinkholes and the Engineering and Environmental Impacts of Karst* (pp. 288-302).
- Katz, B.G., Chelette, A.R. and Pratt, T.R., 2004. Use of chemical and isotopic tracers to assess nitrate contamination and ground-water age, Woodville Karst Plain, USA. *Journal of Hydrology*, *289*(1-4), pp.36-61.
- Katz, B.G., 2004. Sources of nitrate contamination and age of water in large karstic springs of Florida. *Environmental Geology*, *46*(6), pp.689-706.
- Kendall, C. and Aravena, R., 2000. Nitrate isotopes in groundwater systems. In *Environmental tracers in subsurface hydrology* (pp. 261-297). Boston, MA: Springer US.
- Kincaid, T.R., Hazlett, T.J. and Davies, G.J., 2005. Quantitative groundwater tracing and effective numerical modeling in karst: an example from the Woodville Karst Plain of North Florida. In *Sinkholes and the engineering and environmental impacts of karst* (pp. 114-121).
- Kuniansky, E.L., 2016. *Simulating groundwater flow in karst aquifers with distributed parameter models—comparison of porous-equivalent media and hybrid flow approaches* (No. 2016-5116). US Geological Survey.
- Pellerin, B.A., Bergamaschi, B.A., Downing, B.D., Saraceno, J.F., Garrett, J.D. and Olsen, L.D., 2013. *Optical techniques for the determination of nitrate in environmental waters: Guidelines for instrument selection, operation, deployment, maintenance, quality assurance, and data reporting* (No. 1-D5). US Geological Survey.
- Richmond, K., Flesher, C., Lindzey, L., Tanner, N. and Stone, W.C., 2018, October. SUNFISH®: A human-portable exploration AUV for complex 3D environments. In *OCEANS 2018 MTS/IEEE Charleston* (pp. 1-9). IEEE.

- Richmond, K., Flesher, C., Tanner, N., Siegel, V. and Stone, W.C., 2020, October. Autonomous exploration and 3-D mapping of underwater caves with the human-portable SUNFISH® AUV. In *Global Oceans 2020: Singapore–US Gulf Coast* (pp. 1-10). IEEE.
- Ronayne, M.J., 2013. Influence of conduit network geometry on solute transport in karst aquifers with a permeable matrix. *Advances in water resources*, *56*, pp.27-34.
- Scanlon, B.R., Mace, R.E., Barrett, M.E. and Smith, B., 2003. Can we simulate regional groundwater flow in a karst system using equivalent porous media models? Case study, Barton Springs Edwards aquifer, USA. *Journal of hydrology*, *276*(1-4), pp.137-158.
- Shoemaker, W.B., Kuniansky, E.L., Birk, S., Bauer, S. and Swain, E.D., 2008. *Documentation of a conduit flow process (CFP) for MODFLOW-2005* (Vol. 6). Reston, Va: US Department of the Interior, US Geological Survey.
- Snow, D.D., Cassada, D.A., Bartelt–Hunt, S.L., Li, X., Zhang, Y., Zhang, Y., Yuan, Q. and Sallach, J.B., 2012. Detection, occurrence and fate of emerging contaminants in agricultural environments. *Water Environment Research*, *84*(10), pp.764-785.
- Worthington, S.R., Schindel, G.M. and Alexander, C.E.J., 2001. Aquifer scale properties for hydraulic characterization of carbonate aquifers. *Geol. Surv. Am., Abs. Programs, A-411*.